

A DESIGN CRITERION
FOR ARBITRARY DIFFUSERS

Donald Robert Gapp

United States Naval Postgraduate School



THESIS

A DESIGN CRITERION
FOR ARBITRARY DIFFUSERS

by

Donald Robert Gapp

June 1970

This document has been approved for public release and sale; its distribution is unlimited.

1134525

—

A Design Criterion for Arbitrary Diffusers

by

Donald Robert Gapp
Lieutenant, United States Navy
B.S., South Dakota School of Mines and Technology, 1960

Submitted in partial fulfillment of the
requirements for the degree of

AERONAUTICAL ENGINEER

from the

NAVAL POSTGRADUATE SCHOOL
June 1970

ABSTRACT

This study presents the derivation of a diffuser design parameter, which takes into account losses due to the geometry of the diffuser.

A criterion for design of annular diffusers, using the design parameter to predict losses, is developed from reference data and model tests.

A curved wall annular diffuser was designed and tested to verify the predictions of the design criterion for an arbitrary diffuser.

TABLE OF CONTENTS

I.	INTRODUCTION	13
II.	DEVELOPMENT OF THE SHAPE PARAMETER OMEGA (Ω)	16
	A. ENTROPY CHANGE OF A ONE-DIMENSIONAL, FRICTIONAL FLOW . .	16
	B. ENTROPY CHANGE FROM THERMODYNAMIC CONSIDERATIONS	19
	C. DEFINITION OF OMEGA (Ω)	21
	D. RELATIONS BETWEEN Ω AND DIFFUSER PERFORMANCE	22
III.	TEST INSTALLATION AND INSTRUMENTATION	26
	A. AIR DELIVERY SYSTEM	26
	B. DESCRIPTION OF DIFFUSER MODELS AND ASSEMBLY	28
	C. INSTRUMENTATION	33
IV.	COMPUTATIONS AND EXPERIMENTAL PROCEDURES	38
	A. PRESSURE	38
	B. TEMPERATURE	38
	C. FLOW RATE	39
	D. CHECK OF NOZZLE FLOW RATE WITH SURVEY DATA	40
	E. REYNOLDS NUMBER	44
V.	ANALYSIS OF TEST DATA FROM REFERENCE 2	45
VI.	DISCUSSION OF TEST DATA	48
VII.	CONCLUSIONS AND RECOMMENDATIONS	60
	APPENDIX A - Determination of Diffuser Efficiency	61
	APPENDIX B - Design of Diffuser Model (2)	63
	APPENDIX C - Computer Program Omega	67
	C1 - Assembly of Input Data	67
	C2 - Output	68
	APPENDIX D - Reduction of Data from Sovran and Klomp, Reference 2 .	75

BIBLIOGRAPHY	80
FORM DD 1473	83

LIST OF TABLES

Table		Page
I	Diffuser descriptions	35
II	Model (1) and Model (2) test data	51
III	Meridional static pressure values for Model (1) and Model (2)	58
C1	Listing of Program Omega	70
C2	Sample output of Program Omega	74
D1	Listing of reference data reduction program	76
D2	Sovran and Klomp, GMR-511, data	77

LIST OF ILLUSTRATIONS

Figure		Page
1	Example of diffusers which previously had the same description	14
2	One-dimensional flow in a diverging channel	17
3	T-s diagram for an adiabatic, polytropic compression in a stationary duct	20
4	Schematic of the air delivery system	27
5	Transition ducting, looking downstream	29
6	Support assembly, including support struts	29
7	Diffuser support assembly and converging outer wall (with Model (1) attached)	30
8	Diffuser support assembly with Model (1) cantilevered center-body installed	30
9	Center-body of Model (2)	31
10	Outer wall of Model (2) with support assembly	31
11	Schematic of diffuser assembly	32
12	Schematic of diffuser Model (1)	34
13	Overall view of the experimental apparatus	36
14	Diffuser inlet plane, velocity survey in radial direction (measured by hot-wire anemometer)	41
15	Diffuser inlet plane, velocity survey in radial direction (measured by five-hole pressure probe)	42
16	$\bar{\Omega} \bar{c}_f$ vs. Ω for Reference 2 data	46
17	$\bar{\Omega} \bar{c}_f$ vs. Ω , Model (1) test data	49
18	Comparison of Reference 2 data with Model (1) and Model (2) test data	50
19	Diffuser polytropic efficiency vs. Reynolds number	54

20	Dimensionless pressure distribution along outer wall of Model (1)	55
21	Dimensionless pressure distribution along the inner and outer walls of Model (2)	56
22	Design of Model (2)	64
23	Fitting of circular arcs	65
24	Input field specifications for Program Omega	69

LIST OF SYMBOLS

Symbol	Definition	Units
A	Area	in^2
C	Wetted perimeter	in^2
C_{pr}	Coefficient of pressure recovery	---
C_{pri}	Ideal coefficient of pressure recovery	---
c_f	Local coefficient of friction	---
$\overline{c_f}$	Average local coefficient of friction	---
c_p	Specific heat of air at constant pressure	$\text{BTU/lb}_m - ^\circ\text{R}$
d	Distance from outer wall	in
g_c	Unit conversion factor	$\text{ft-lb}_m/\text{lb-sec}^2$
K	Texas Instrument pressure gauge conversion factor	in $\text{H}_2\text{O}/\text{count}$
L	Axial length	in
\overline{L}	Meridional length along mean streamline	in
\overline{L}_w	Meridional wall length	in
\overline{l}	Meridional length along wall	in
M	Mach number	---
\dot{m}	Mass flow rate	slugs/sec
\dot{m}_{lr}	Referred mass flow rate	---
mV	Temperature reading	millivolts
n	Polytropic exponent	---
P_t	Total pressure, absolute	lb/in^2
p	Static pressure, absolute	lb/in^2
Δp	Pressure difference between two points in the flow	lb/in^2

q	Dynamic pressure ($P_t - p$)	lb/in^2
R_g	Gas constant	$\text{ft} - \text{lb/lb}_m - ^\circ\text{R}$
R_e	Reynolds number	---
s	Entropy	---
T_t	Total temperature	$^\circ\text{R}$
T	Static temperature	$^\circ\text{R}$
t_c	Temperature	$^\circ\text{C}$
t_f	Temperature	$^\circ\text{F}$
V	Average velocity	ft/sec
\dot{w}	Flow rate	lb_m/sec
w^*	Equivalent flow rate	in^2
x	Factor $(p_u - p_d)/p_d$	---
γ	Ratio of specific heats	---
ϵ	Density coefficient	---
ζ	Dimensionless static pressure	---
η_p	Polytropic efficiency	---
λ	Dimensionless length	---
μ	Viscosity	$\text{lb}_m - \text{sec/ft}^2$
ρ	Density	slugs/ft^3
τ	Wall shear stress	lb/ft^2
Φ_c	Flow function	---
Ω	Shape parameter	---

Subscripts

1	Station at diffuser inlet plane
1r	Referred to station one
2	Station at diffuser exit plane
A	Atmospheric

d	Downstream from nozzle
H	Hub or inner wall
is	Isentropic
p	Polytropic
T	Tip or outer wall
TI	Values measured on the Texas Instrument Fused Quartz Pressure Gage
t	Total
u	Upstream from nozzle
w	At or along wall

ACKNOWLEDGEMENT

The author wishes to acknowledge the guidance given by Professor M. H. Vavra of the Department of Aeronautics of the Naval Postgraduate School, and assistance of Mr. James E. Hammer and the technical staff of the Turbopropulsion Laboratory in the preparation of the experimental portion of this thesis.

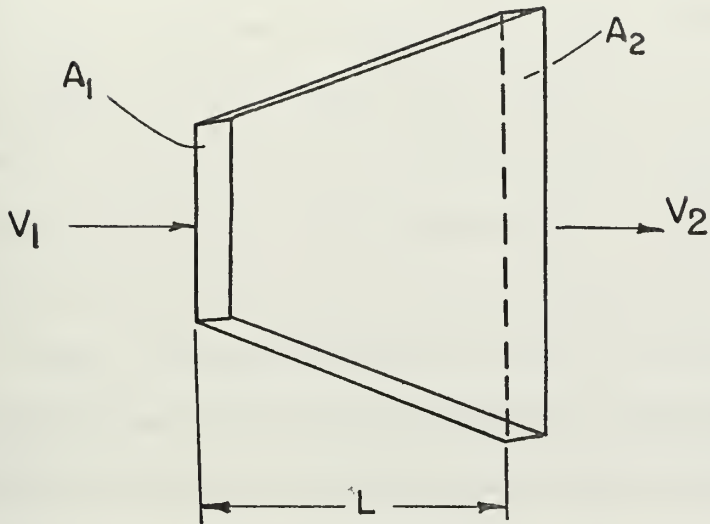
Special thanks go to Mr. Gordon Gulbranson, non-metal model maker of the Department of Aeronautics for the beautiful diffuser models which he fabricated.

I. INTRODUCTION

In the design of annular diffusers, such as those found in jet engines, and turbomachines, there has been a problem defining parameters which indicate sufficiently the optimum design range for varying geometries. Many schemes have been devised, such as the so-called "equivalent conical angle method", to relate a diffuser to a known shape. The difficulty in these approaches has been that each person using the method developed a slightly different approach which resulted in a variety of descriptions for the same diffuser. Gleason [1] gives a summary of such methods and points out the difficulty in correlating data from different sources.

Some apparent problems arise when describing a diffuser by inlet area, exit area, length, difference in inlet radii, equivalent cone angle, or combinations of these parameters developed by empirical means. Although these terms give some intuitive feel for the way a diffuser would perform, two diffusers which differ widely in performance could have the same definition.

The simple example of Figure 1, where the two diffusers have the same inlet area, exit area, length and possibly the same divergence angle, makes it immediately obvious that the two diffusers would not have the same losses. The velocity and pressure distributions through the diffuser channel have a direct effect on the boundary layer development, which in turn controls the frictional losses. The widely differing geometries of the two above-mentioned diffusers would cause large differences in boundary layer growth. Therefore,



$$A_1 = A_1' \quad , \quad A_2 = A_2' \quad , \quad L = L' \quad , \quad L/A_1 = L'/A_1' \quad ,$$

$$V_1 = V_1' \quad \quad V_2 \neq V_2'$$

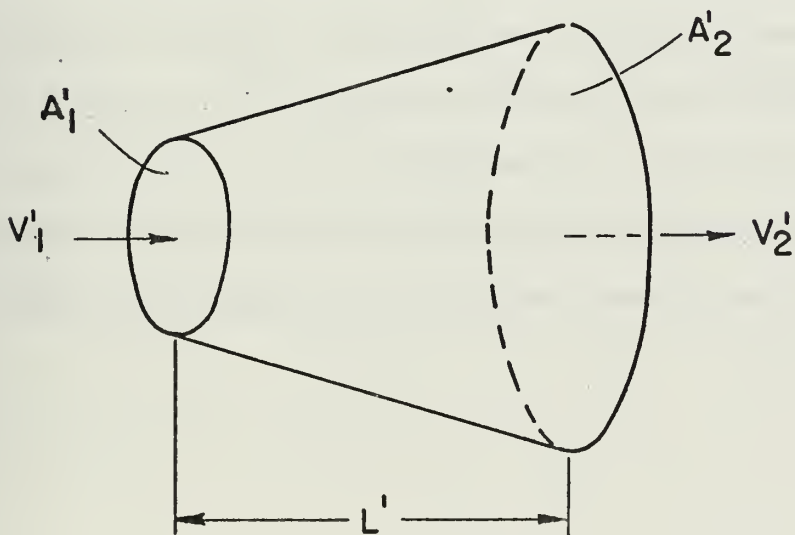


FIGURE 1

Example of diffusers which previously had the same description.

the performance of the two would differ and a similar description would not be appropriate.

Sovran and Klomp [2] have empirically developed a fairly successful set of parameters for straight wall annular diffusers. The geometric area ratio was taken as the primary factor affecting diffusion, and a non-dimensionalized length when combined with the area ratio, gave an overall criterion for the pressure-gradient affecting the boundary layer development. Their description of annular diffusers is at present limited to designs with straight walls.

Vavra [3 and 4] presented the idea of a shape factor or parameter which includes the effects of diffusion and boundary layer influence for the evaluation and preliminary design of diffusers of arbitrary shapes.

The objectives of this study were to present the derivation of the shape parameter, Ω , to substantiate its usefulness from reference data, and to evaluate the validity of the results by construction and investigation of a family of straight wall diffusers such as those in Ref. 2. To show that the design shape parameter may be applied to diffusers other than those with straight walls, a curved wall diffuser such as might be found at the exit of the high pressure compressor of a jet engine was designed for an optimum Ω and evaluated by tests.

II. DEVELOPMENT OF THE SHAPE PARAMETER OMEGA (Ω)

The function of a diffuser is to convert a portion of the kinetic energy of the free stream into static pressure by a compression process similar to that in a mechanical compressor. The shape parameter, Omega (Ω), to be used for diffuser design, can be evolved by examining the differential entropy changes of such a polytropic compression process.

A. ENTROPY CHANGE OF A ONE-DIMENSIONAL, FRICTIONAL FLOW

An expression for the differential entropy change of a polytropic compression may be found by investigating a one-dimensional flow in a diverging channel, such as shown in Fig. 2. A momentum balance on the differential volume of Fig. 2 gives

$$\dot{m} (V + dV) - \dot{m}V = pA - (p + dp) (A + dA) + (p + dp/2) dA - \tau C dL$$

(1)

which reduces to

$$\dot{m} dV = -Adp - \tau C dL$$

(2)

or

$$dp = -\frac{\dot{m}}{A} dV - \frac{\tau C}{A} dL$$

(3)

where the values of A, C, p, dL, V, and τ are as defined in Fig. 2.

Introducing the equation of continuity,

$$\dot{m} = \rho VA$$

(4)

into equation (3) results in

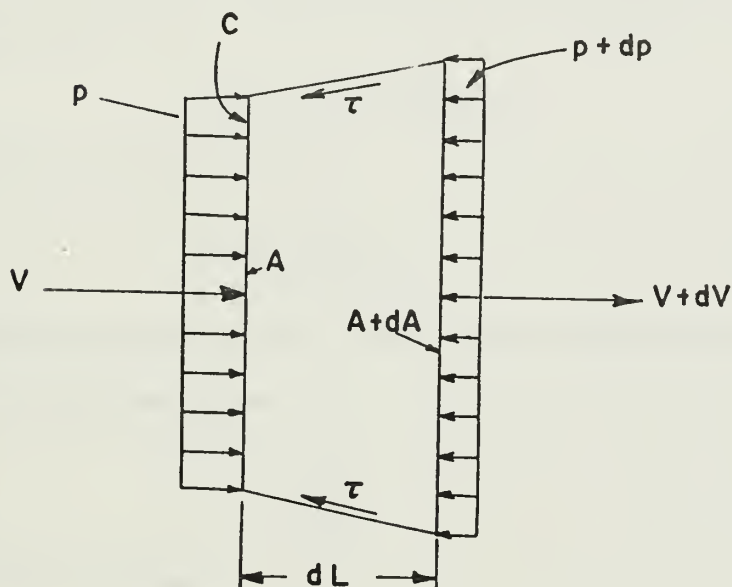
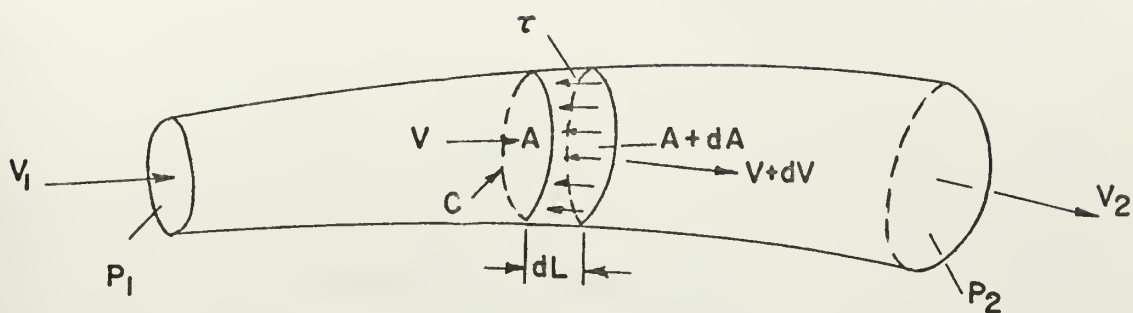
$$dp = -\rho V dV - \frac{\tau C dL}{A}$$

(5)

or

$$\frac{dp}{\rho} = -d(V^2/2) - \frac{\tau}{\rho} \frac{C}{A} dL$$

(6)



A = Flow Cross-Sectional Area
 C = Wetted Perimeter
 p = Static Pressure
 V = Average Velocity
 τ = Wall Shear Stresses
 L = Meridional Length

FIGURE 2

One-dimensional flow in a diverging channel.

with the First Law of Thermodynamics

$$dq = du + pdv = dh - vdp = dh - \frac{1}{\rho} dp = Tds \quad (7)$$

or

$$\frac{dp}{\rho} = dh - Tds \quad (8)$$

Equating (6) and (7) gives

$$dh + d(V^2/2) - Tds = \frac{\tau}{\rho} \frac{C}{A} dL \quad (9)$$

The first two terms of (9) combine to the derivative of the total enthalpy, H , and if the flow is restricted to an adiabatic case, with no energy in any form transferred between the fluid and its surroundings, the total enthalpy is constant and its derivative is equal to zero.

Therefore,

$$dH = d(h + V^2/2) = 0$$

and equation (8) simplifies to

$$Tds = \frac{\tau}{\rho} \frac{C}{A} dL \quad (10)$$

Introducing the concept of the local coefficient of skin friction in a one-dimensional flow,

$$c_f \equiv \frac{\tau}{1/2\rho V^2} \quad (11)$$

equation (10) becomes

$$Tds = \frac{c_f}{2} V^2 \frac{C}{A} dL \quad (12)$$

Introducing equation (4) and the equation of state for a perfect gas in (12) results in an expression for the differential entropy change,

$$ds = \frac{c_f}{2} \frac{\dot{m}^2}{\rho^2 A^3} \frac{C}{T} dL = \frac{c_f}{2} \frac{\dot{m}^2}{\rho} \frac{R}{p} \frac{C}{A^3} dL \quad (13)$$

B. ENTROPY CHANGE FROM THERMODYNAMIC CONSIDERATIONS

The differential change in entropy can also be found for an adiabatic, polytropic compression process as shown in the T-s diagram of Fig. 3. The definition of polytropic efficiency is,

$$\eta_p \equiv \frac{dT_{is}}{dT} \quad (14)$$

The isentropic relation for a differential compression from p to p + dp is

$$\frac{T + dT_{is}}{T} = \left(\frac{p + dp}{p} \right)^{\frac{\gamma-1}{\gamma}} \quad (15)$$

By expanding (dp/p) by a binomial series, and assuming dp to be small compared to p,

$$dT_{is} \doteq T \frac{\gamma-1}{\gamma} \frac{dp}{p} \quad (16)$$

Combining (14) and (16) gives

$$dT = \frac{T}{\eta_p} \frac{\gamma-1}{\gamma} \frac{dp}{p} \quad (17)$$

Solving equation (7) for

$$ds = c_p \frac{dT}{T} - \frac{1}{\rho T} dp$$

and introducing

$$c_p = R_g \frac{\gamma}{\gamma-1}$$

and the perfect gas law

$$p/\rho = R_g T$$

results in an expression for

$$ds = R_g \left[\frac{\gamma}{\gamma-1} \frac{dT}{T} - \frac{dp}{p} \right] \quad (18)$$

Substituting (17) into (18) gives

$$ds = R_g \frac{dp}{p} \left[\frac{1}{\eta_p} - 1 \right] \quad (19)$$

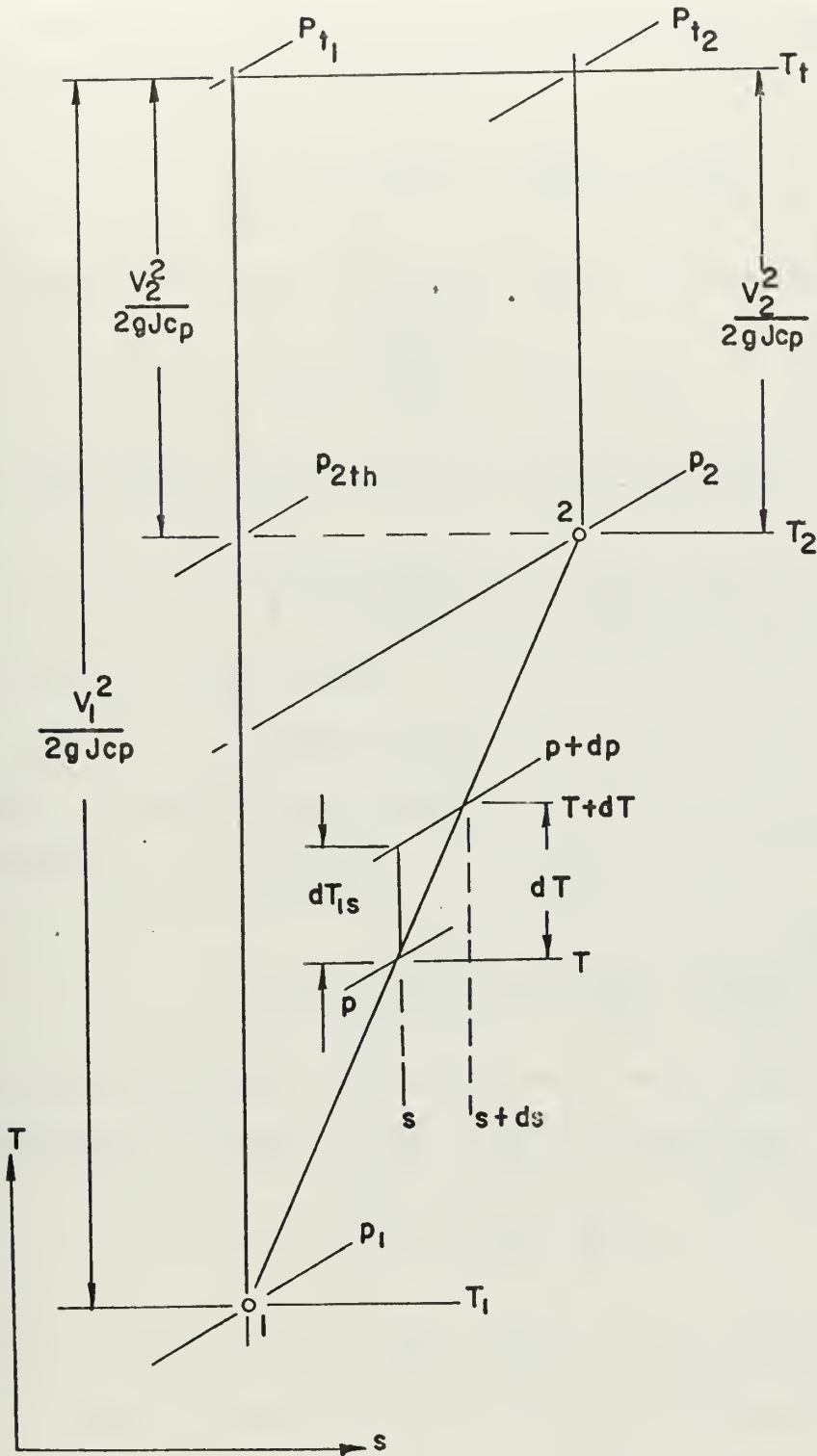


FIGURE 3

T-s diagram for an adiabatic, polytropic compression in a stationary duct.

C. DEFINITION OF OMEGA (Ω)

Equating the two values of differential entropy change from equations (13) and (19) results in

$$\frac{c_f}{2} \frac{\dot{m}}{\rho} \frac{C}{A^3} \frac{R_g}{p} dL = \frac{R_g}{p} \left[\frac{1}{\eta_p} - 1 \right] dp \quad (20)$$

Introducing the concept of referred flow rate, a dimensionless quantity,

$$\dot{m}_{lr} \equiv \frac{\sqrt{R_g T_1}}{p_1 A_1} \dot{m} \quad (21)$$

and substituting (21) into (20) and rearranging gives

$$\frac{c_f}{2} \dot{m}_{lr}^2 \left(\frac{A_1}{A} \right)^3 \frac{C}{A_1} dL = \left[\frac{1}{\eta_p} - 1 \right] \frac{\rho}{\rho_1} d \left(\frac{p}{p_1} \right) \quad (22)$$

For a polytropic process

$$p/\rho^n = \text{constant}$$

where n is the polytropic exponent.

Rewriting (22) in the form

$$\frac{c_f}{2} \dot{m}_{lr}^2 \left(\frac{A_1}{A} \right)^3 \frac{C}{A_1} dL = \left[\frac{1}{\eta_p} - 1 \right] \left(\frac{p}{p_1} \right)^{1/n} d \left(\frac{p}{p_1} \right) \quad (23)$$

gives two independent differentials which can be integrated.

Defining the left side of (23) as dX_1 and integrating,

$$X_1 = \int_0^{\bar{L}} \frac{c_f}{2} \dot{m}_{lr}^2 \left(\frac{A_1}{A} \right)^3 \frac{C}{A_1} dL \quad (24)$$

where \bar{L} is the meridional length along the mean streamline.

Assuming an average value of coefficient of friction, \bar{c}_f , for the whole surface and that \dot{m}_{lr} is a constant for a given flow rate, (24) may be rewritten as

$$X_1 = \frac{\bar{c}_f}{2} \dot{m}_{1r}^2 \int_0^{\bar{L}} \left(\frac{A_1}{A}\right)^3 \frac{C}{A_1} dL \quad (25)$$

The integral of (25) is a parameter which contains the flow area ratio, the diffuser length, and the wetted surface, and will be called the "diffuser shape parameter", defined by

$$\Omega \equiv \int_0^{\bar{L}} \left(\frac{A_1}{A}\right)^3 \frac{C}{A_1} dL \quad (26)$$

D. RELATIONS BETWEEN Ω AND DIFFUSER PERFORMANCE

Defining the right-side of (23) as dX_2 ,

$$X_2 = \int_1^{P_2/P_1} \left[\frac{1}{\eta_p} - 1 \right] \left(\frac{P}{P_1} \right)^{1/n} d \left(\frac{P}{P_1} \right) \quad (27)$$

If η_p and n are assumed constant,

$$X_2 = \left[\frac{1}{\eta_p} - 1 \right] \frac{1}{(1/n + 1)} \left[\left(\frac{P_2}{P_1} \right)^{(1/n + 1)} - 1 \right] \quad (28)$$

For

$$P_2 = P_1 + \Delta p$$

the binominal expansion

$$\begin{aligned} \left(\frac{P_2}{P_1} \right)^{1/n + 1} &= \left(\frac{P_1 + \Delta p}{P_1} \right)^{1/n + 1} = \left(1 + \frac{\Delta p}{P_1} \right)^{1/n + 1} \\ &= 1 + \left(\frac{1}{n} + 1 \right) \frac{\Delta p}{P_1} + \dots \end{aligned}$$

Assuming Δp is much less than P_1 and omitting higher order terms from the binomial expansion, equation (28) becomes

$$X_2 = \left[\frac{1}{\eta_p} - 1 \right] \frac{\Delta p}{P_1} \quad (29)$$

Equating X_1 and X_2 ,

$$\left[\frac{1}{\eta_p} - 1 \right] \frac{\Delta p}{p_1} = \frac{\bar{c}_f}{2} \dot{m}_{lr}^2 \Omega \quad (30)$$

With the equation of continuity, equation (21) becomes

$$\dot{m}_{lr} = \rho_1 V_1 A_1 \frac{\sqrt{R_g T}}{p_1 A_1} \quad (31)$$

Substituting \dot{m}_{lr} into equation (30)

$$\left[\frac{1}{\eta_p} - 1 \right] \frac{\Delta p}{1/2 \rho_1 V_1^2} = \bar{c}_f \Omega \quad (32)$$

For a constant total temperature, equation (18) becomes

$$ds = - R_g \frac{dP_t}{P_t}$$

Thus equation (19) becomes

$$- \frac{dP_t}{P_t} = \left[\frac{1}{\eta_p} - 1 \right] \frac{dp}{p} \quad (33)$$

Integrating (33)

$$\ln \left(\frac{P_{t1}}{P_{t2}} \right) = \left[\frac{1}{\eta_p} - 1 \right] \ln \left(\frac{p_2}{p_1} \right) \quad (34)$$

Using the assumption that $P_{t2} = P_{t1} + \Delta P_t$ and $p_2 = p_1 + \Delta p$, where ΔP_t and Δp are small compared to P_t and p , respectively, and with the truncated power series expansion of $\ln(1+x) \doteq x$, (34) becomes

$$\frac{\Delta P_t}{P_{t1}} = \left[\frac{1}{\eta_p} - 1 \right] \frac{\Delta p}{p_1}$$

or

$$\left[\frac{1}{\eta_p} - 1 \right] \Delta p = \Delta P_t \left(\frac{p_1}{P_{t1}} \right) = \Delta P_t \frac{1}{1 + \frac{\gamma}{2} M_1^2} \quad (35)$$

Since for an incompressible flow, M^2 , is small compared to unity,

$$\left[\frac{1}{\eta_p} - 1 \right] \Delta p = \Delta p_t \quad (36)$$

Substituting (36) into (32) gives

$$\bar{c}_f \Omega = \frac{\Delta p_t}{1/2 \rho_1 v_1^2} \quad (37)$$

In Ref. 2, the Pressure Recovery Coefficient is defined as the ratio of the actual pressure rise and the maximum attainable one for the particular flow rate, or

$$C_{pr} \equiv \frac{p_2 - p_1}{1/2 \rho_1 v_1^2} \quad (38)$$

Defining the Ideal Pressure Recovery Coefficient as that which would result for an isentropic compression producing the theoretical pressure $p_{2_{th}}$ of Fig. 3,

$$C_{pri} \equiv \frac{p_{2_{th}} - p_1}{1/2 \rho_1 v_1^2} \quad (39)$$

For isentropic flow $\Delta p_t = 0$, and assuming density to be constant and introducing the equation of continuity,

$$C_{pri} = \frac{\rho/2 v_1^2 - \rho/2 v_2^2}{\rho/2 v_1^2} = 1 - \left(\frac{A_1}{A_2} \right)^2 \quad (40)$$

From equation (40),

$$\rho/2 v_2^2 = \rho/2 v_1^2 [1 - C_{pri}]$$

Then

$$p_{t_1} - p_{t_2} = p_1 + \rho/2 v_1^2 - p_2 - \rho/2 v_1^2 [1 - C_{pri}]$$

or

$$\frac{P_{t_1} - P_{t_2}}{\rho/2 V_1^2} = \frac{P_1 - P_2}{\rho/2 V_1^2} + C_{pri} \quad (41)$$

Using the definition of C_{pr} , (38), and equation (37) there is

$$\bar{\Omega} c_f = C_{pri} - C_{pr} \quad (42)$$

or

$$\bar{c}_f = \frac{C_{pri} - C_{pr}}{\Omega} \quad (43)$$

Hence, after having previously determined Ω , the average frictional loss coefficient, \bar{c}_f , can be calculated from the measured quantities p_1 , q_1 , A_1 , p_2 , and A_2 .

III. TEST INSTALLATION AND INSTRUMENTATION

The apparatus used in this investigation was located in Building 230 at the Turbopropulsion Laboratories of the Department of Aeronautics, Naval Postgraduate School, Monterey, California.

A. AIR DELIVERY SYSTEM

A schematic drawing of the installation is shown in Fig. 4. The air source was a 200 H.P., Carrier centrifugal compressor with a maximum flow rate of about four pounds mass of air per second at a pressure ratio of about two. Gross throttling was accomplished by a main by-pass valve ahead of the air coolers. Fine adjustments of the flow rate were made by bleeding air from plenum (1) through a secondary by-pass valve.

The air from plenum (1) discharged through a flow straightener into a four inch pipe containing a flow measuring nozzle. The nozzle used was the same as that described by Kelly [5], which had a diameter of 3.022 inches and a diameter ratio, β , of 0.734.

The flow was diffused into plenum (2) by a ten degree conical diffuser extending downward from the inlet. The discharge of plenum (2) was into a rectangular wooden duct containing flow straighteners and a total temperature, iron-constantan thermocouple probe.

The mean stream velocity in the duct at maximum flow rate was approximately 20 to 25 feet per second. Transition pieces shown in Fig. 5 were used to change the geometry of the flow channel from rectangular to circular and to accelerate the flow to the diffuser inlet velocity and pressure.

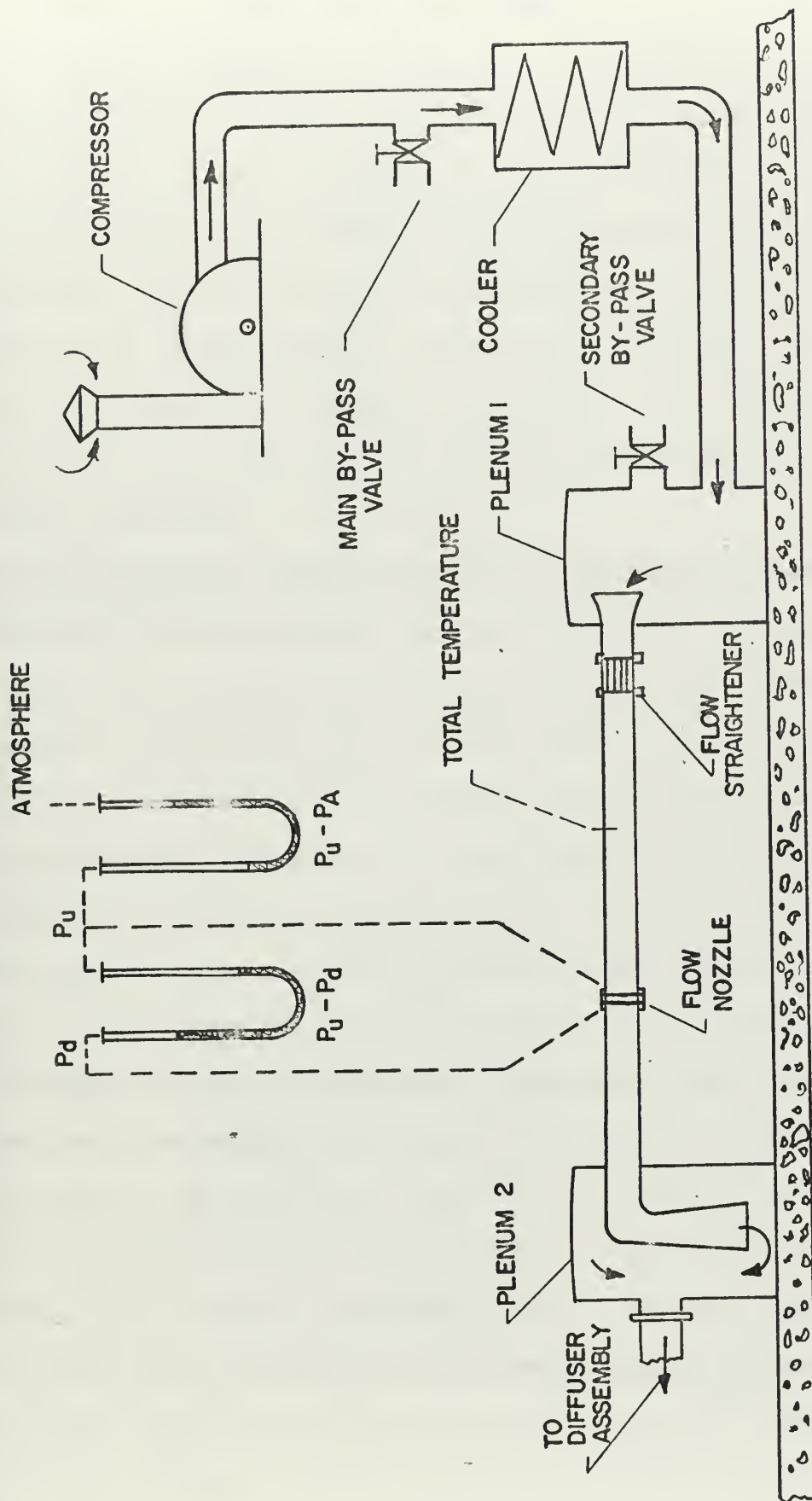


FIGURE 4

Schematic of the air delivery system.

B. DESCRIPTION OF DIFFUSER MODELS AND ASSEMBLY

The diffuser assemblies of the two models constructed and their supporting assembly are shown in the photographs of Figures 6 through 10. The supporting assembly consisted of the duct transition pieces with a cylindrical portion, shown in Fig. 6, containing three equally spaced support struts for a cantilevered center-body, so that no obstructions or supports would be necessary in the diffuser flow channel. The flow was accelerated to the diffuser entrance in an annular space created by the nose of the center-body assembly and a converging outer wall.

A straight section, where the annular area remained constant, was provided just downstream of the inlet to provide room for flow measurements and surveys, as shown in the schematic of Fig. 11. Smooth transitions to the diffuser contour were arranged as shown in Figures 8 and 9. All computations of the diffuser shape parameter included the flow area from the inlet plane to the exit plane of the diffuser, inclusive of the cylindrical inlet section.

The diffuser inlet plane was provided with three supports for probes, equally spaced around the outer periphery and bisecting the angles formed by the supporting struts of the center-body. These supports could accommodate both hot-wire and pressure probes for radial surveys. One support was used for a Kiel probe for the measuring of total pressure at the inlet plane. Three static pressure taps were provided in the same plane, 120 degrees apart on the outer wall. Three sets of static taps were placed axially downstream from the inlet static taps, at two-inch intervals on the outer wall of the first model, and on both the inner and outer walls at one-inch intervals on the second

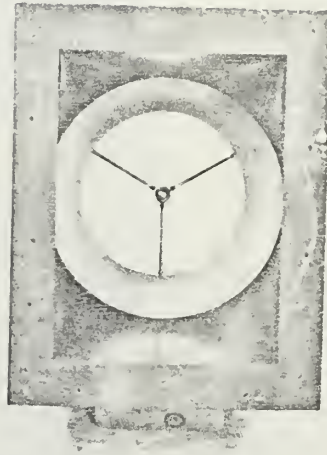


FIGURE 5

Transition ducting, looking downstream.

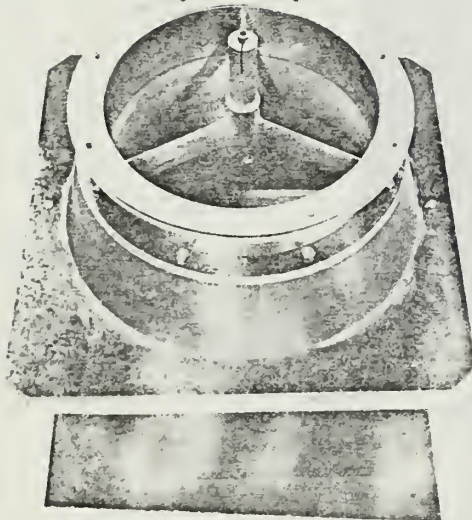


FIGURE 6

Support assembly, including support struts.

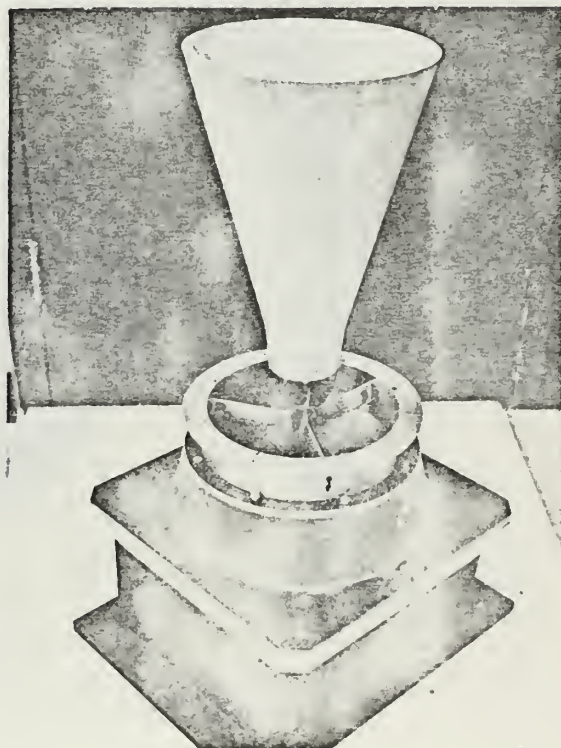


FIGURE 7

Diffuser support assembly and
converging outer wall (with
Model (1) attached).

FIGURE 8

Diffuser support assembly with
Model (1) cantilevered center-body
installed.



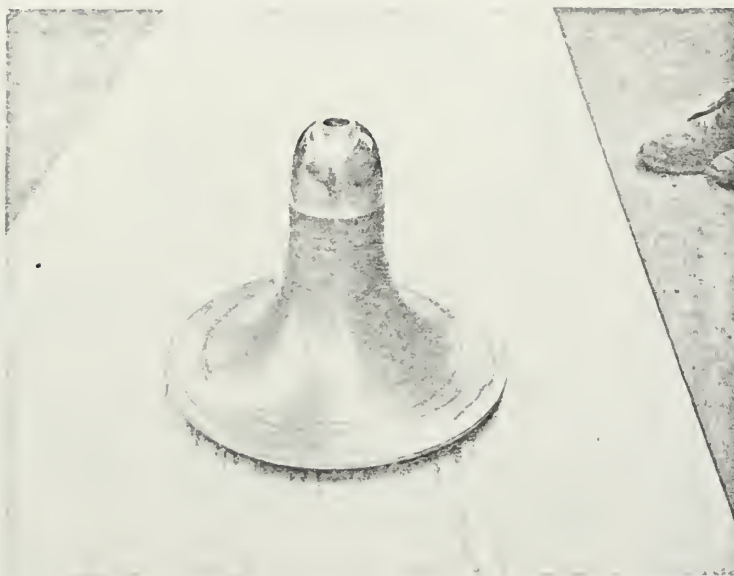


FIGURE 9

Center-body of Model (2)

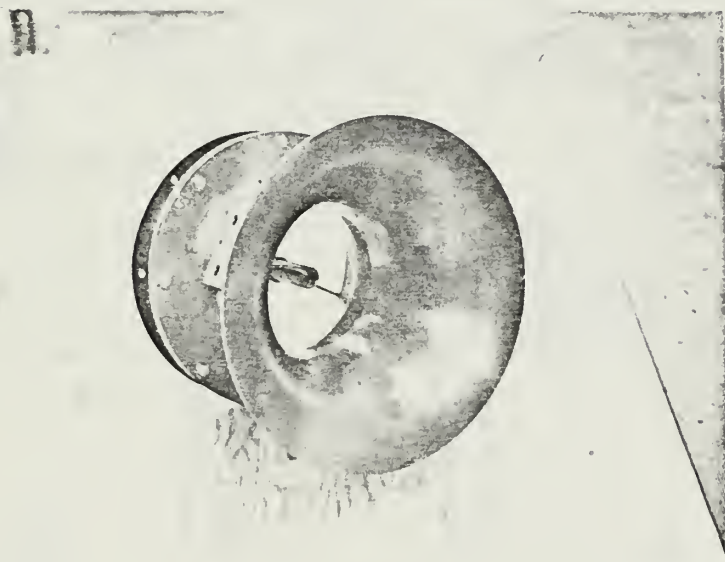


FIGURE 10

Outer wall of Model (2) with Support Assembly.

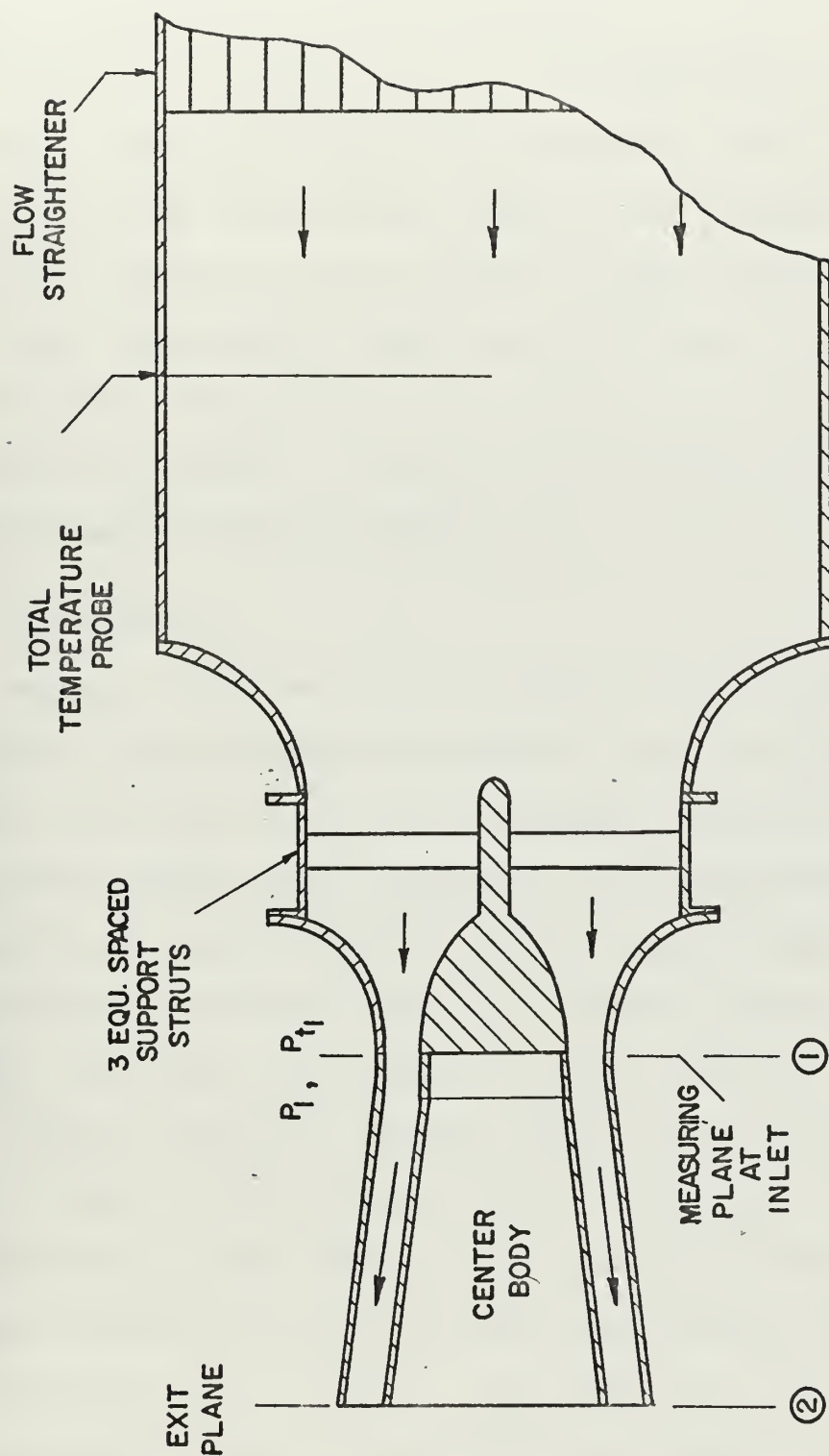


FIGURE 11
Schematic of diffuser assembly.

model. Static pressure readings were found to be equal at all three stations around the circumference, and the three taps at each axial location were therefore connected together.

Model (1) had straight walls as illustrated in Fig. 12, with a wall divergence angle of 15 degrees for both the inner and outer contours. The construction was such that a series of four diffusers with different shape parameters could be produced by simply cutting off the end of the model. Model (2) had a more complicated shape, and was designed as described in Appendix B to show the validity of the Ω parameter for curved-wall diffusers. A summary of the geometrical characteristics of both models is given in Table I.

C. INSTRUMENTATION

Pressure readings for the flow nozzle and the diffuser inlet were made with a Texas Instrument Fused Quartz Pressure Gage, which is shown in the overall view of the experimental apparatus of Fig. 13. A constant pressure source calibration of the Pressure Gage, to a Meriam Vernier Manometer filled with water, gave a constant value of 0.800 inches of water per count, with a reading accuracy of ± 0.001 counts. This result was identical to that of Beck [6].

Pressure readings for five-hole probe measurements were made on a 235 cm, eight tube water manometer bank, which can be read to an accuracy of ± 0.1 cm. Static pressure measurements along the diffuser length were made on a 92 inch, 20 tube water manometer board with a reading accuracy of ± 0.05 inch. All pressure taps were connected to their respective reading devices with plastic tubing. A standard mercury wall-barometer was used for atmospheric pressure readings.

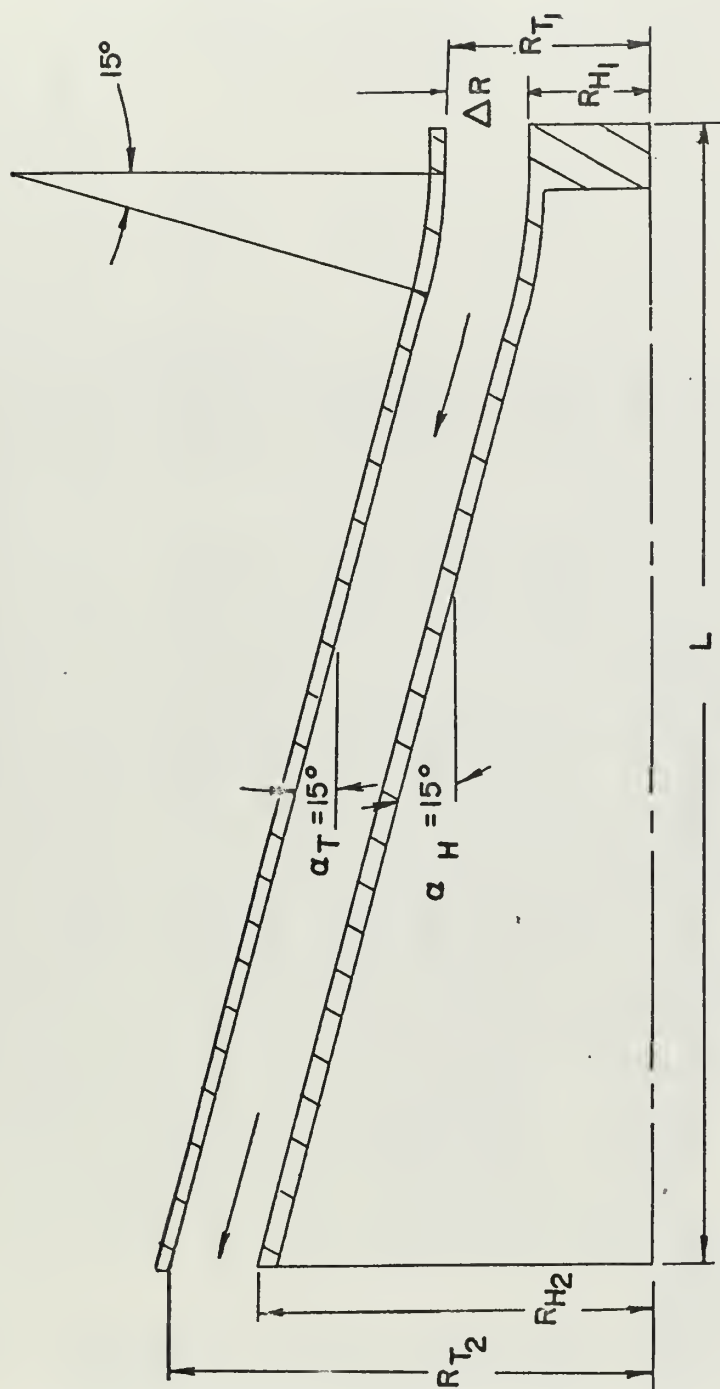


FIGURE 12
Schematic of diffuser Model (1)

TABLE I
Diffuser Descriptions

Model	Configuration	R_{H1} Inches	R_{T1} Inches	A_1 Inches ²	A_2 Inches ²	L Inches	Ω	Material
1	1	1.875	3.123	19.596	50.232	15.0	11.521	Phenolic Resin **
1	2	1.875	3.123	19.596	40.076	10.0	9.689	"
1	3	1.875	3.123	19.596	33.582	7.0	8.012	"
1	4	1.875	3.123	19.596	29.140	5.0	6.470	"
2	1	1.875	3.123	19.596	43.980	8.56*	5.701	Epolute Resin**

* Meridional length along mean streamline (\bar{L})

** Rezolin Brand

See Fig. 12 for description of dimensions.

See Section II for definition of Ω

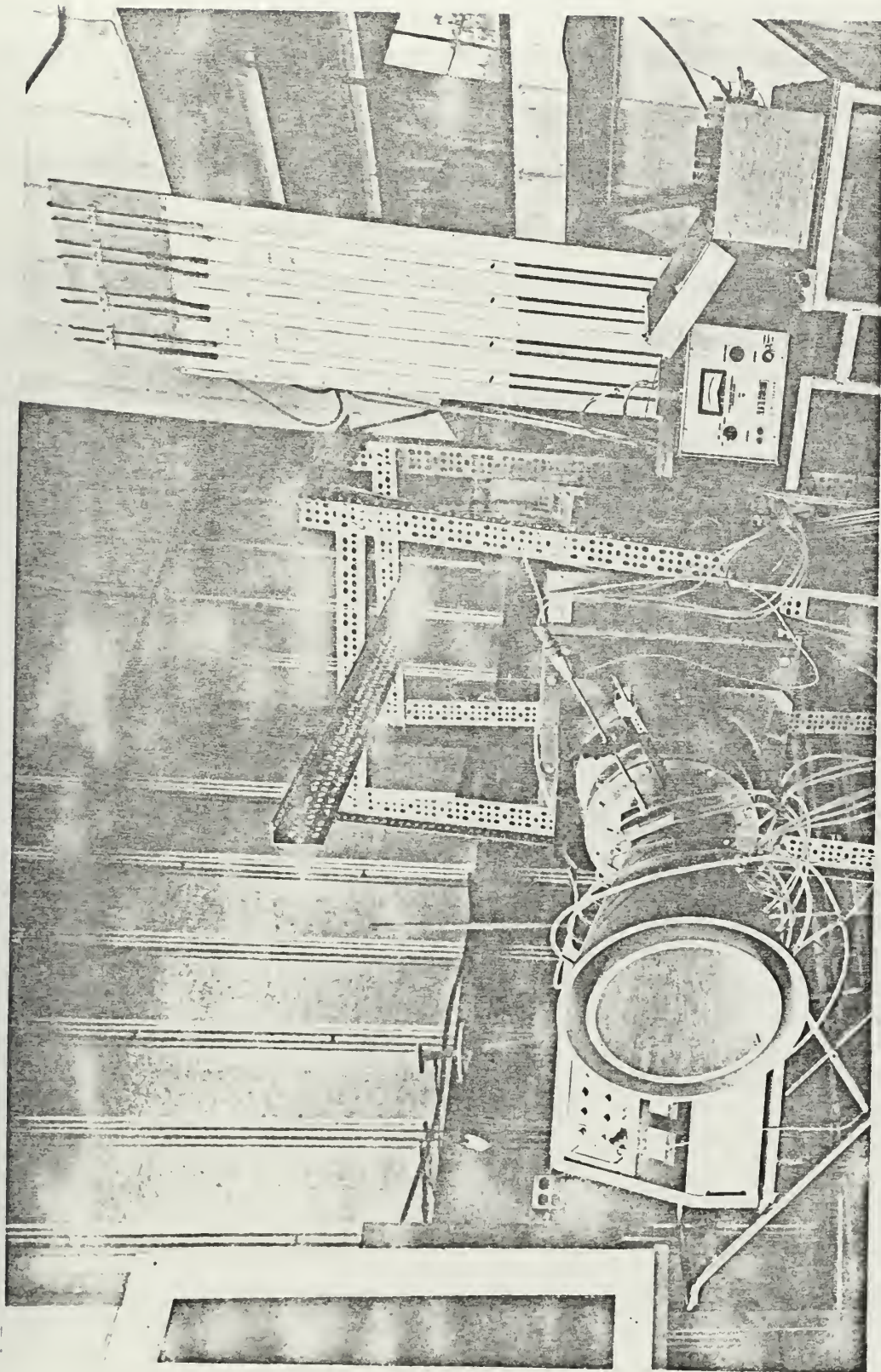


FIGURE 13
Overall view of the experimental apparatus.

Temperature readings from the thermocouples upstream of the flow nozzle, and in the wooden duct, were obtained with a Leeds and Northrup portable potentiometer with compensated cold-junction, giving a reading accuracy of ± 0.01 mV. Adiabatic flow was assumed from the area of temperature measurement to that of pressure measurement.

Hot-wire measurements were conducted with a two channel, constant temperature, hot-wire anemometer manufactured by Applied Science, Carmel, California. The wires were 0.00015 inch diameter tungsten with a 0.1 inch gap. Surveys were taken radially from the outer to the inner wall.

IV. EXPERIMENTAL PROCEDURES AND COMPUTATIONS

All reduction of data was carried out by the Fortran IV computer program "Omega" described in Appendix C.

A. PRESSURE

Pressures obtained from the Texas Instrument Fused Quartz Pressure Gage were reduced to pounds per square inch by

$$p = 0.03613 K p_{TI} \quad (44)$$

where $K = 0.8$, the conversion factor from counts to inches of water, p_{TI} is the pressure read in counts on the Pressure Gage, and the constant value, 0.03613, is the conversion factor for inches of water to pounds per square inch from Ref. 7.

Barometric pressure was converted from inches of mercury to pounds per square inch by equation (3-2) of Ref. 6.

$$p_A = 0.4912 p \left[1 - \frac{0.0001634 t_c}{1 + 0.0001818 t_c} \right] \quad (45)$$

where the coefficients of t_c , the room temperature in degrees centigrade, are the thermal expansion coefficients of mercury and brass. The factor 0.4912 is the conversion factor for inches of mercury at 0°C to pounds per square inch from Ref. 7.

B. TEMPERATURE

Thermocouple readings, recorded in millivolts, were converted to degrees Fahrenheit by the temperature relationship,

$$t_f = 32.144 + 35.77 \text{ mV} - 0.4518 \text{ mV} \quad (46)$$

obtained from a least squares fit of data from Ref. 8. This relation holds for temperatures below 100 degrees Fahrenheit, with the cold-junction maintained at 32 degrees, or compensated to 32 degrees by the standard cell of the Leeds and Northrup measuring apparatus.

C. FLOW RATE

After setting the desired flow rate, the fluid temperatures were allowed to stabilize before data were taken. Upstream static pressure, p_u , differential pressure across the flow nozzle, $(p_u - p_d)$, and the upstream total temperature, t_{fu} , are necessary to compute flow rate as described in Appendix A of Ref. 5.

$$\dot{w} = \frac{\dot{w}^*}{\sqrt{t_{fu}}} \sqrt{\frac{p_u}{R_g}} \quad (47)$$

and

$$\dot{w}^* = 11.30 \epsilon f_t \sqrt{\frac{p_u - p_d}{p_u}} \quad (48)$$

where \dot{w}^* is the equivalent flow rate, which has dimension in^2 .

The so-called expansion coefficient, ϵ , is

$$\epsilon = \sqrt{2.433 \frac{(1-x)^{1.428}}{x} \left[\frac{1 - (1-x)^{0.286}}{1 - .305(1-x)^{1.428}} \right]} \quad (49)$$

where

$$x = \frac{p_u - p_d}{p_u} \quad (50)$$

and

$$f_t = 1 / 0.0015 \left(\frac{t_{fu} - 60}{100} \right) \quad (51)$$

is a correction factor that takes account of the thermal expansion of the nozzle throat diameter.

D. CHECK OF NOZZLE FLOW RATE WITH SURVEY DATA

Preliminary surveys at the inlet plane with a hot-wire probe indicated that the velocity profiles at the three stations surveyed were similar. Figure 14 is a least-squares fit of the data points from all three survey stations. The data were taken at varying flow rates at each station, and the velocities were found to vary within ± 1 per cent of the mean obtained with the least-square fit. Hence, the flow was very nearly axisymmetric, and the non-dimensional profiles remained unchanged at the different flow rates investigated. The boundary layer was very thin at the inlet. The actual thicknesses were 0.025 inch on the inner wall and 0.75 inch on the outer wall according to the measurements.

To verify the pressure and temperature measurements, a comparison was made of the flow obtained from the survey data at the inlet and that measured by the flow nozzle. A survey with a five-hole probe was made at the inlet plane to obtain the actual values of the velocities which are plotted in Fig. 15. Data for the five-hole probe were corrected by use of the calibration curves supplied by the manufacturer, United Sensor and Control Corporation. The velocity profile obtained was essentially the same as that of the hot-wire surveys. The hot-wire values were used for the boundary layer regions, where the immersion corrections for the pressure probe were unreliable. The yaw angles of the flow were less than $\pm 1/2^\circ$, and the flow had pitch angles between three and six degrees, with the velocities pointing outward from the center. The greatest velocities occurred at the outer wall.

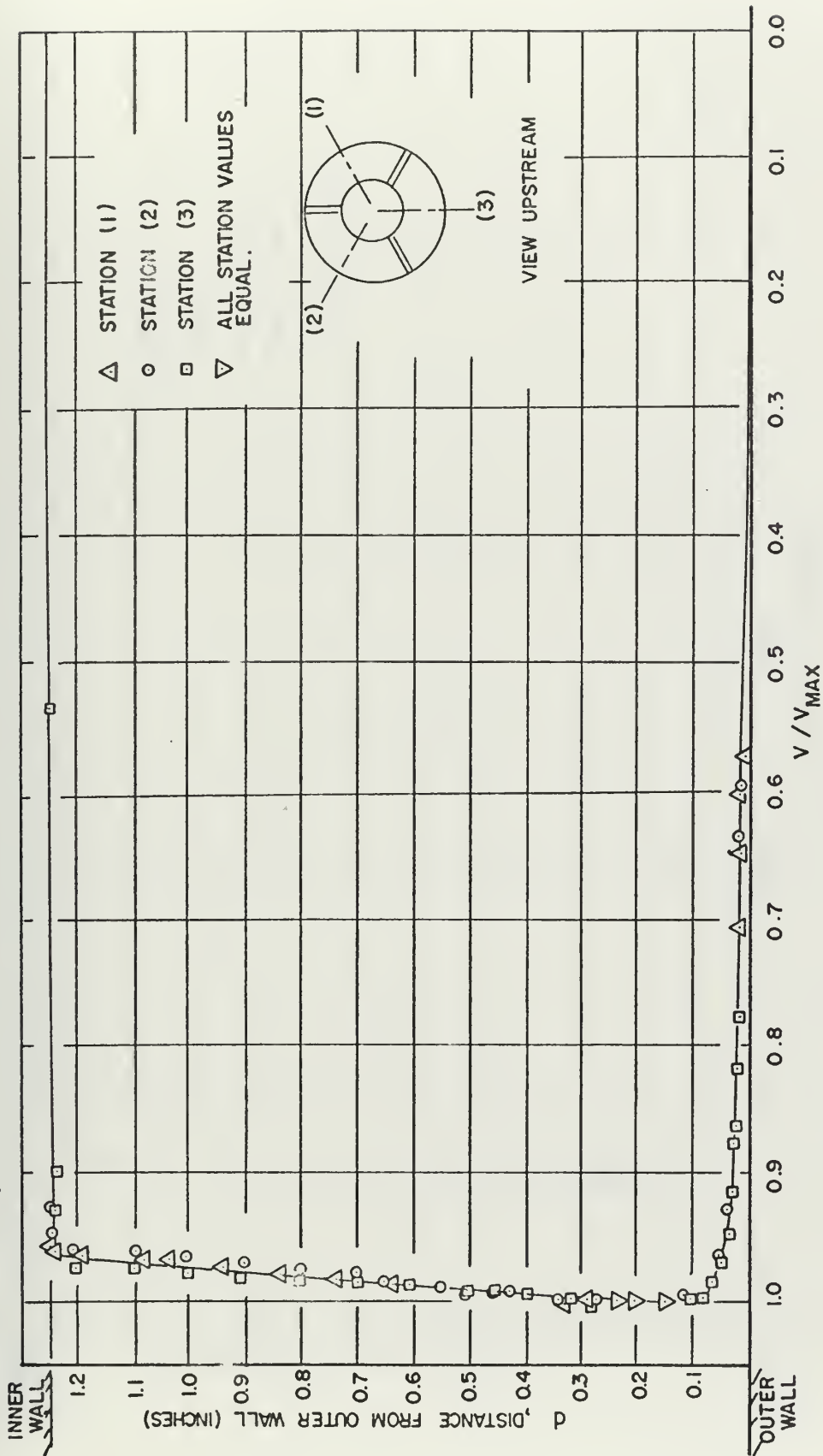


FIGURE 14

Diffuser inlet plane, velocity survey in radial direction (measured by hot-wire anemometer).

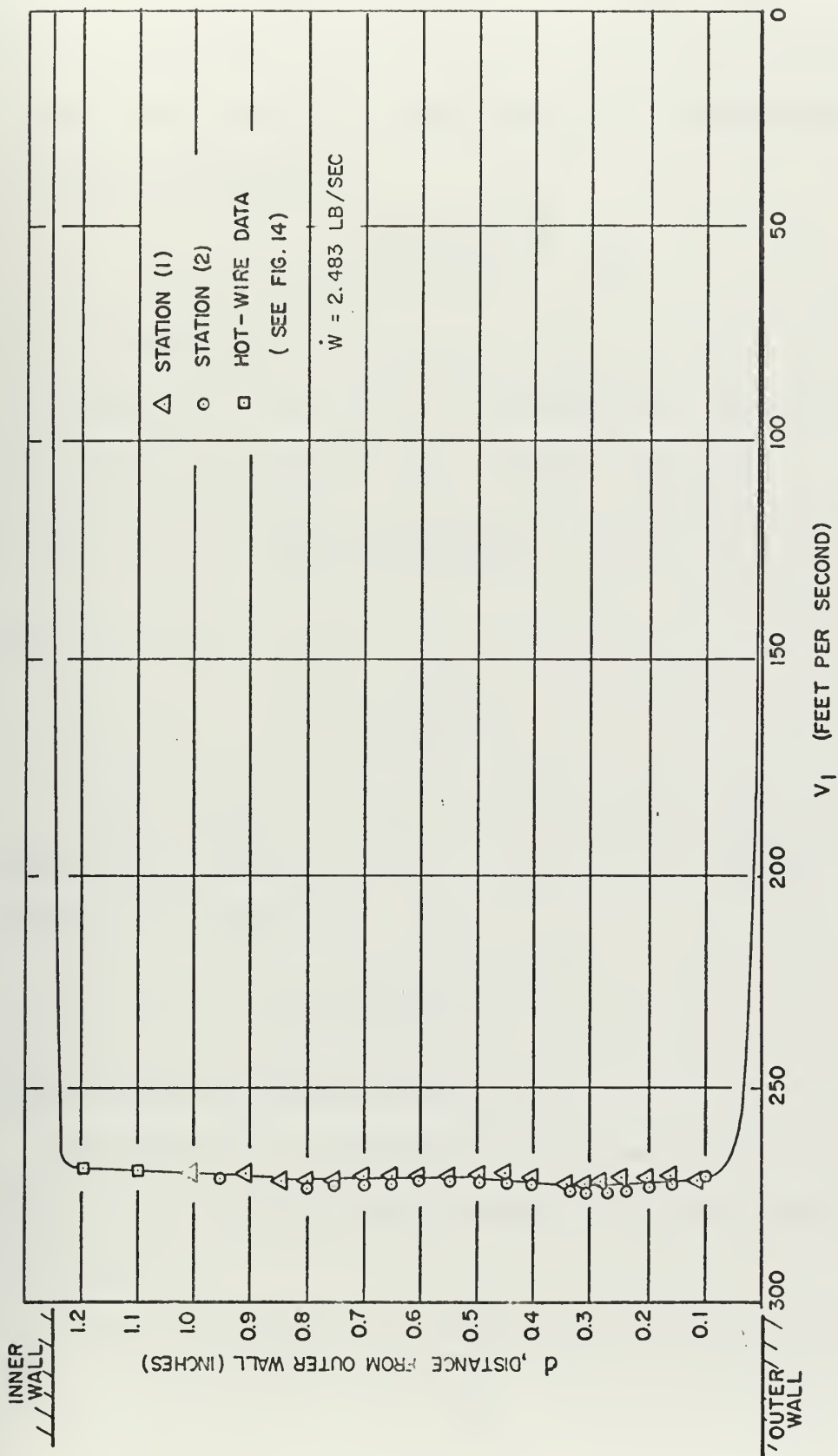


FIGURE 15

Diffuser inlet plane, velocity survey in radial direction (measured by five-hole pressure probe).

The five-hole probe survey showed the total pressures and the velocities to be within two per cent of the mean values in the turbulent central region outside the boundary layers. An average Mach number of the flow in this central region was determined from the isentropic relationship

$$M_1 = \left\{ \frac{2}{\gamma-1} \left[\left(\frac{P_{t1}}{P_1} \right)^{\frac{\gamma-1}{\gamma}} - 1 \right] \right\}^{1/2} \quad (52)$$

The average static temperature at the inlet was determined by assuming adiabatic flow from the upstream total temperature probe to the inlet plane, which gave the isentropic relationship

$$\frac{T_{t1}}{T_1} = 1 + \frac{\gamma-1}{2} M_1^2 \quad (53)$$

Hence,

$$T_1 = \frac{T_{t1}}{1 + \frac{\gamma-1}{2} M_1^2} \quad (54)$$

Static pressure was found to be nearly uniform across the inlet plane, so that density was almost constant at this station. From the perfect gas relationship,

$$\rho_1 = \frac{p_1 (144)}{R_g g_c T_1} \quad (55)$$

with the units of slugs per cubic foot.

From the survey, the velocities were known as a function of radius, $V(r)$. Thus, a flow rate was calculated at the inlet plane by numerical integration of

$$\dot{w}_1 = 2 \pi \rho_1 \int_{R_{H1}}^{R_{T1}} V(r) r dr \quad (56)$$

assuming axisymmetric flow and no blockage from support strut wakes. This flow rate was found to be three to four per cent higher than the flow rate obtained from the flow nozzle measurements. This comparison was considered satisfactory for the range of measuring capability.

E. REYNOLDS NUMBER

The characteristic length for the Reynolds number (Re) was taken as the hydraulic radius of the inlet annulus, ΔR_1 , as in Ref. 2, or

$$\Delta R_1 = \frac{2 \text{ (flow area)}_1}{\text{(wetted perimeter)}_1} \quad (57)$$

Therefore,

$$Re = \frac{\rho_1 V_1 \Delta R_1}{\mu} \quad (58)$$

and, substituting

$$\dot{w} = \rho_1 V_1 A_1 = \rho_1 V_1 \pi (R_{T1}^2 - R_{H1}^2) \quad (59)$$

the Reynolds number (Re) can be expressed in dimensionally correct units as

$$Re = \frac{\dot{w} (12)}{g \mu \pi (R_{T1} + R_{H1})} \quad (60)$$

where viscosity, μ , has a representative value of 3.9×10^{-7} lb_f-sec/ft² for the operating range of 85 to 95 degrees Fahrenheit. The flow rate, \dot{w} , is in lb_m/sec, and the radii are expressed in inches.

V. ANALYSIS OF TEST DATA FROM REFERENCE 2

Sovran and Klomp [2] made a study of more than one hundred annular diffuser configurations, and their published data was of a form suitable to be analyzed for the present purpose. Of the many other works published, none furnished a sufficiently wide cross-section of data which could be readily applied. Data from Ref. 2 were reduced by the Fortran IV program shown in Table D1. The results are listed in Table D2 and plotted on Fig. 16 for a Reynolds number of approximately 6×10^5 . Each set of data points represents a family of straight wall diffusers having the same inlet area and wall divergence angles as shown in Fig. 16. The data points fall within a band on the plot of $\Omega \bar{c}_f$ versus Ω , which is bounded by lines representing a dimensionless length description of the diffuser, $\bar{L}/\Delta R$. An investigation of the values of $\bar{L}/\Delta R$ for existing diffuser designs indicates that the boundaries shown on Fig. 16 are in the range of practical designs. The points falling below $\bar{L}/\Delta R \doteq 1.5$ represent designs which become so short that diffusion is degraded, and those above $\bar{L}/\Delta R \doteq 13$ become excessively long for practical use. It can be seen, that as Ω falls below approximately five, there is an abrupt rise in the value of $\Omega \bar{c}_f$, which is representative of the entropy rise and thus of an increase of the losses in the diffuser. The trend of the curve for larger values of Ω was found by considering that, as a diffuser with small divergence angles becomes long, its characteristics approach that of a pipe. Reference 9 gives the value of the coefficient of friction for an annular pipe as $\bar{c}_f = 0.01$ at $Re = 6 \times 10^5$. A pipe with $\bar{L}/\Delta R = 13$ has a value of

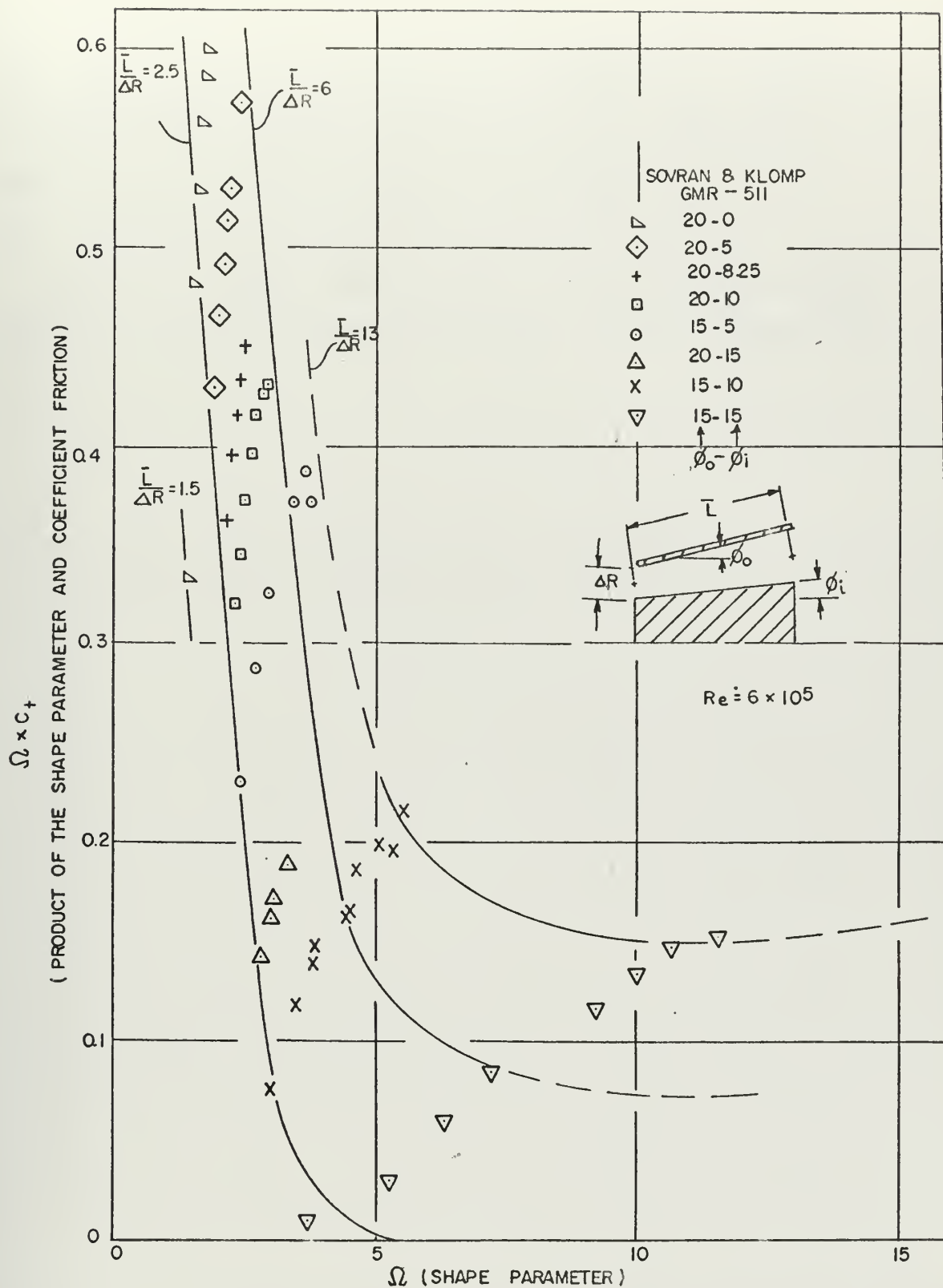


FIGURE 16

$\Omega \bar{c}_f$ vs. Ω for Reference 2 data.

$\Omega = 26$ and $\Omega \bar{c}_f = 0.26$, which is a higher value of $\Omega \bar{c}_f$ than that occurring from diffuser tests at $\Omega = 11.5$ and $\bar{L}/\Delta R = 13$, suggesting an upward trend in the curve for high values of Ω . This trend indicates that a minimum of $\Omega \bar{c}_f$ occurs between about $\Omega = 5$ and $\Omega = 15$, possibly at a value of $\Omega = 10$, for an $\bar{L}/\Delta R = 13$.

Vavra [3] calculated values of $\Omega \bar{c}_f$, for two-dimensional subsonic diffusers, which lie within the same band as the data plotted on Fig. 16.

VI. DISCUSSION OF TEST DATA

The test results obtained from diffuser Model (1) and Model (2) are given in Table II. The quantities $\Omega \bar{c}_f$ for Model (1) are plotted on Fig. 17 versus Ω . Tests were made at different flow rates to investigate the effect of Reynolds number on the location of points in the $\Omega \bar{c}_f$ vs. Ω plot for the different configurations of Model (1). Figure 17 shows that as Reynolds number increases the quantity $\Omega \bar{c}_f$ decreases, and vice versa. This effect could be anticipated from the trend of \bar{c}_f against Re for flows in annular pipes, as shown in Ref. 9.

The curve for $\bar{L}/\Delta R = 6$ and the curve for the family of diffusers with $\Phi_o = \Phi_i = 15^\circ$, from Fig. 16, and the curves from Fig. 17 were transposed to Fig. 18. The shape of the curves from data of Model (1) approximates that of the similar family of diffusers from Fig. 16 for $\Phi_o = \Phi_i = 15^\circ$. However, the values obtained from the tests of Model (1) are considerably lower than those from Ref. 2. This discrepancy may be explained by the fact that the models of Ref. 2 were constructed of wood and, therefore, had a higher wall roughness than the cast resin models used in this study. The value of \bar{c}_f for a wood surface would be larger than that for a resin surface with lower wall roughness, similar to what can be seen from the Moody diagram for pipes of differing roughness.

The values of $\Omega \bar{c}_f$ for configuration four of Model (1) became slightly negative. Values of $\Omega \bar{c}_f$ from Ref. 2 data were also negative when C_{pr} became greater than C_{pri} . For an adiabatic process, the value $\Omega \bar{c}_f$ cannot be negative, since C_{pr} is less than C_{pri} by definition. An investigation of the pressure measurements for configuration four of

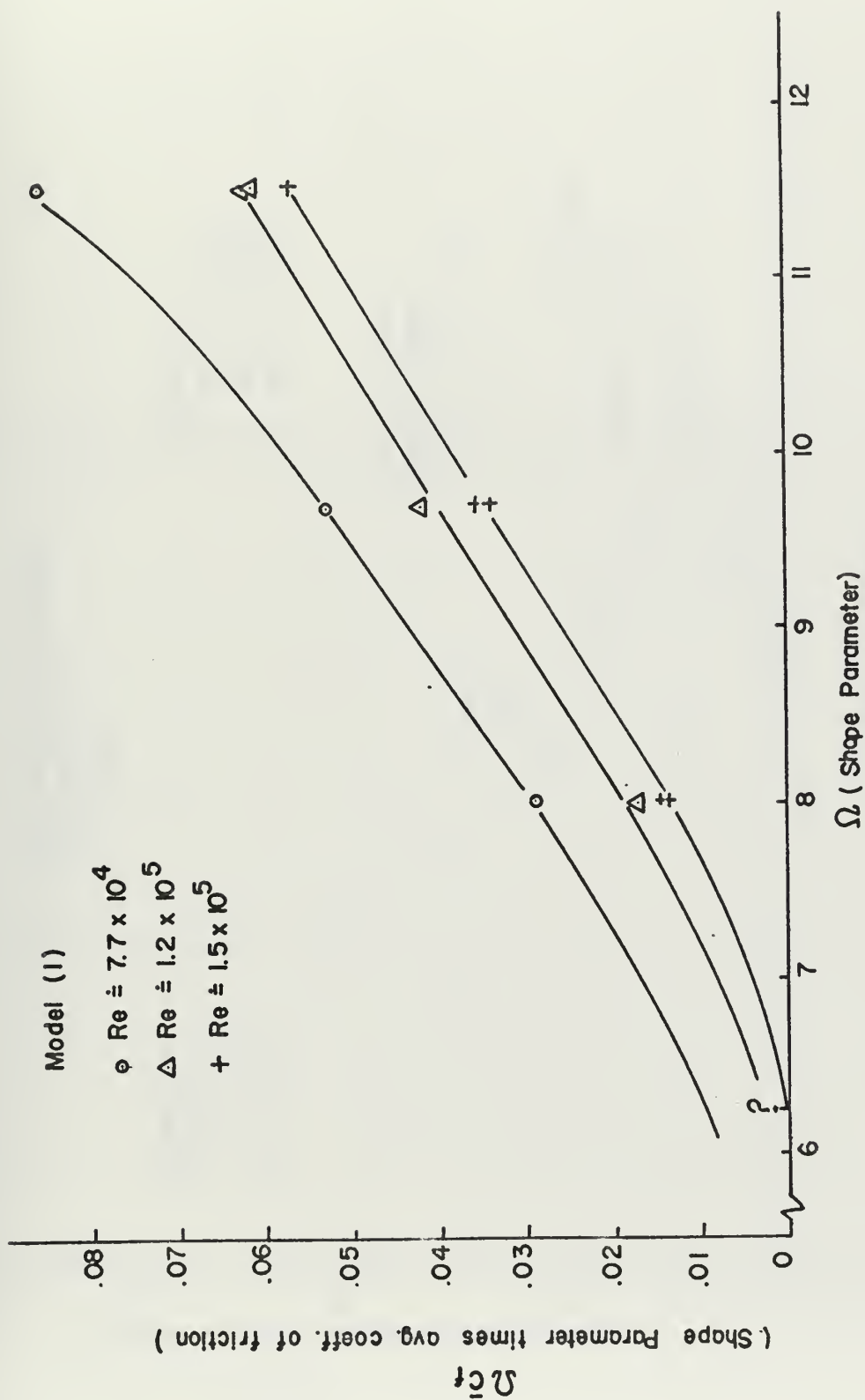


FIGURE 17
 $\Omega \bar{c}_f$ vs. Ω , MODEL (I) test data

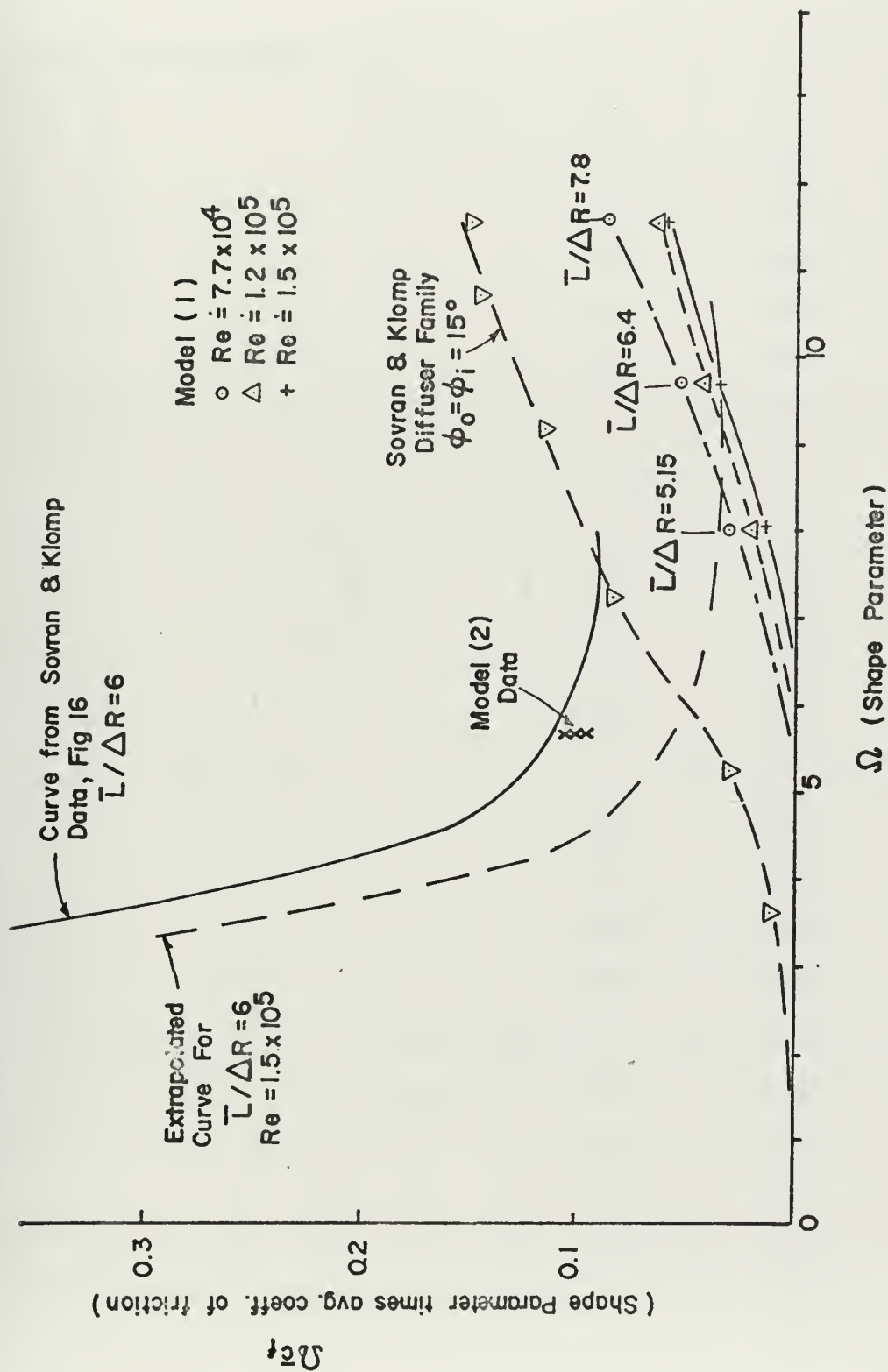


FIGURE 18

Ω_{cf} vs. Ω

Comparison of Reference 2 data with Model (1) and Model (2) test data.

TABLE II

Model (1) and Model (2) test data

MODEL	CONFIGURATION	Ω	$\Omega \bar{c}_f$	η_p	$R_e \times 10^5$
1	1	11.521	0.0614	.8793	1.165
			0.0667	.8837	.879
			0.0566	.8709	1.486
			0.0632	.8628	1.514
			0.0573	.8696	1.518
			0.0569	.8699	1.510
			0.0610	.8794	1.201
			0.0560	.8704	1.526
			0.0859	.8647	.768
	2	9.689	0.0338	.8677	1.517
			0.0356	.8683	1.506
			0.0418	.8734	1.234
			0.0486	.8808	.775
			0.0529	.8740	.762
	3	8.012	0.0288	.8699	.766
			0.0135	.8633	1.509
			0.0170	.8703	1.208
			0.0200	.8780	.980
			0.0146	.8587	1.493
			0.0137	.8607	1.495
	4	6.470	-0.0162	.8589	1.502
			-0.0027	.8756	.755
			-0.0105	.8772	1.034
			-0.0128	.8677	1.265
			-0.0151	.8589	1.494

TABLE II, continued

MODEL	CONFIGURATION	Ω	$\Omega \bar{c}_f$	η_p	$R_e \times 10^5$
2	1	5.701	0.0949	.8226	1.467
			0.1009	.8279	1.143
			0.1036	.8362	.741
			0.0941	.8243	1.466

Model (1) showed a fluctuation of the instrument readings of sufficient magnitude for C_{pr} to be larger than C_{pri} .

It can be anticipated that the curves of Fig. 16 will be shifted vertically up or down with Reynolds number similar to the condition in Fig. 17. The values of Ω for the point of sharply increasing $\Omega \bar{c}_f$ would not be affected by a change in Re , since the entire band of data points would be displaced in the vertical direction only. To avoid large values of $\Omega \bar{c}_f$, a minimum value of $\Omega \doteq 5$ should be used for most practical designs.

To demonstrate the usefulness of the design parameter Ω , for complicated shapes, Model (2) was designed as outlined in Appendix B for a value of $\Omega = 5.7$, and $\bar{L}/\Delta R = 6.85$. Values of $\Omega \doteq 6$ and $\bar{L}/\Delta R \doteq 6$ were chosen for the original design point, to obtain an $\Omega \bar{c}_f \doteq 0.1$.

By extrapolating from the curve for $\bar{L}/\Delta R = 6$ of Fig. 16 to the data of Fig. 17 to show the effect of Re and the difference in the model surfaces, the heavy dashed curve of Fig. 18 was obtained. The data of Model (2), plotted on Fig. 18, verified the location of the $\bar{L}/\Delta R$ curve for an arbitrary shaped diffuser.

The efficiencies for both Model (1) and Model (2), plotted on Fig. 19, remained essentially constant through the Re range of this study.

Static pressure (p_w) on the inner and outer walls of Model (1) and Model (2) was non-dimensionalized by

$$\zeta = \frac{P_{t1} - P_w}{q_1} \quad (61)$$

and plotted against non-dimensionalized, meridional wall length, $\lambda = \bar{l}/\bar{L}_w$, on Figures 20 and 21, where \bar{l} is the meridional distance along the wall from the inlet to the pressure tap, and \bar{L}_w is the

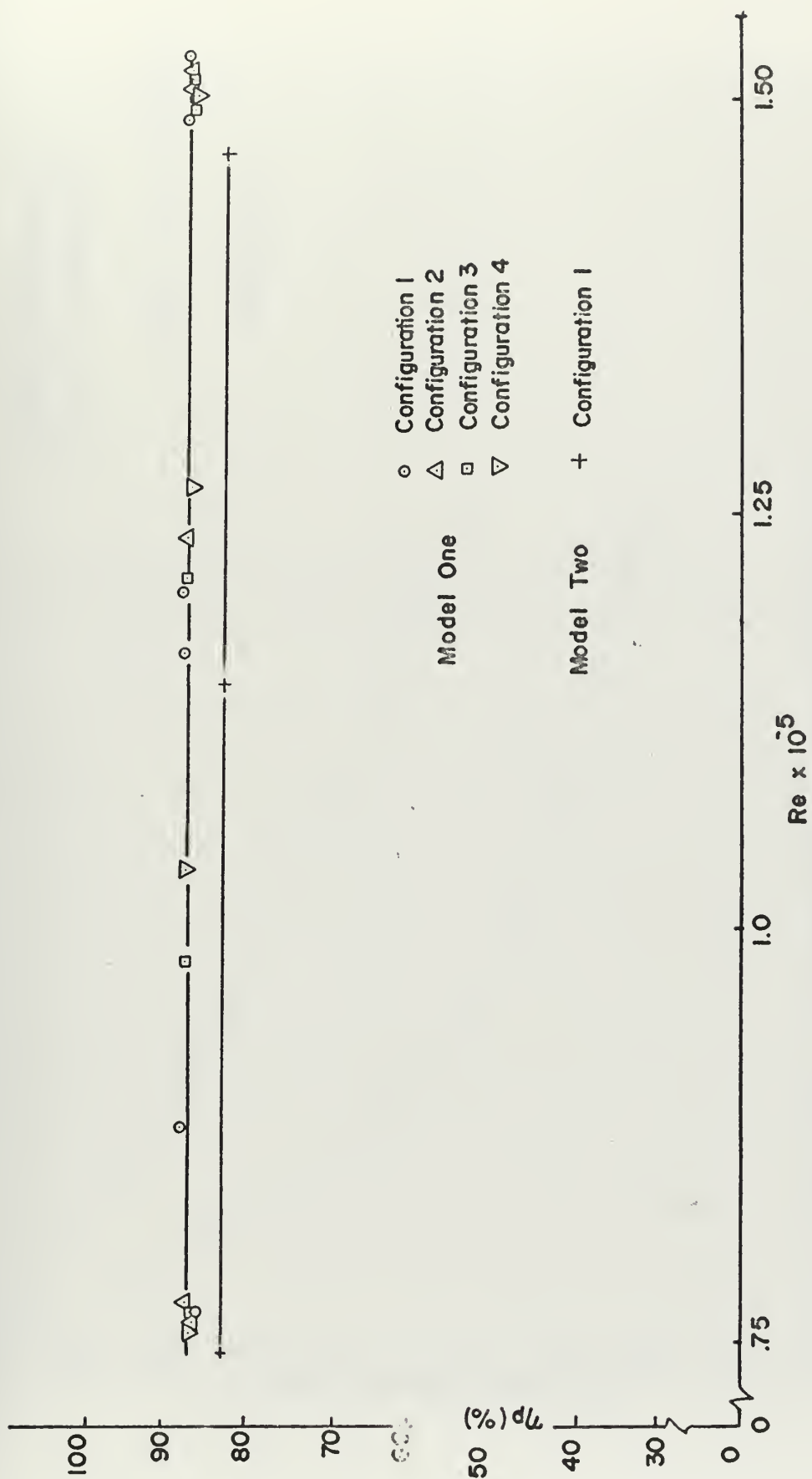


FIGURE 19
DIFFUSER POLYTROPIC EFFICIENCY VS. Re

- Model (I) - Configuration (I)
- △ Model (I) - Configuration (4)

$$\lambda = \frac{\bar{I}}{\bar{L}} \quad , \quad \zeta = \frac{P_{T1} - P_W}{q_1}$$

(See Fig. 21)

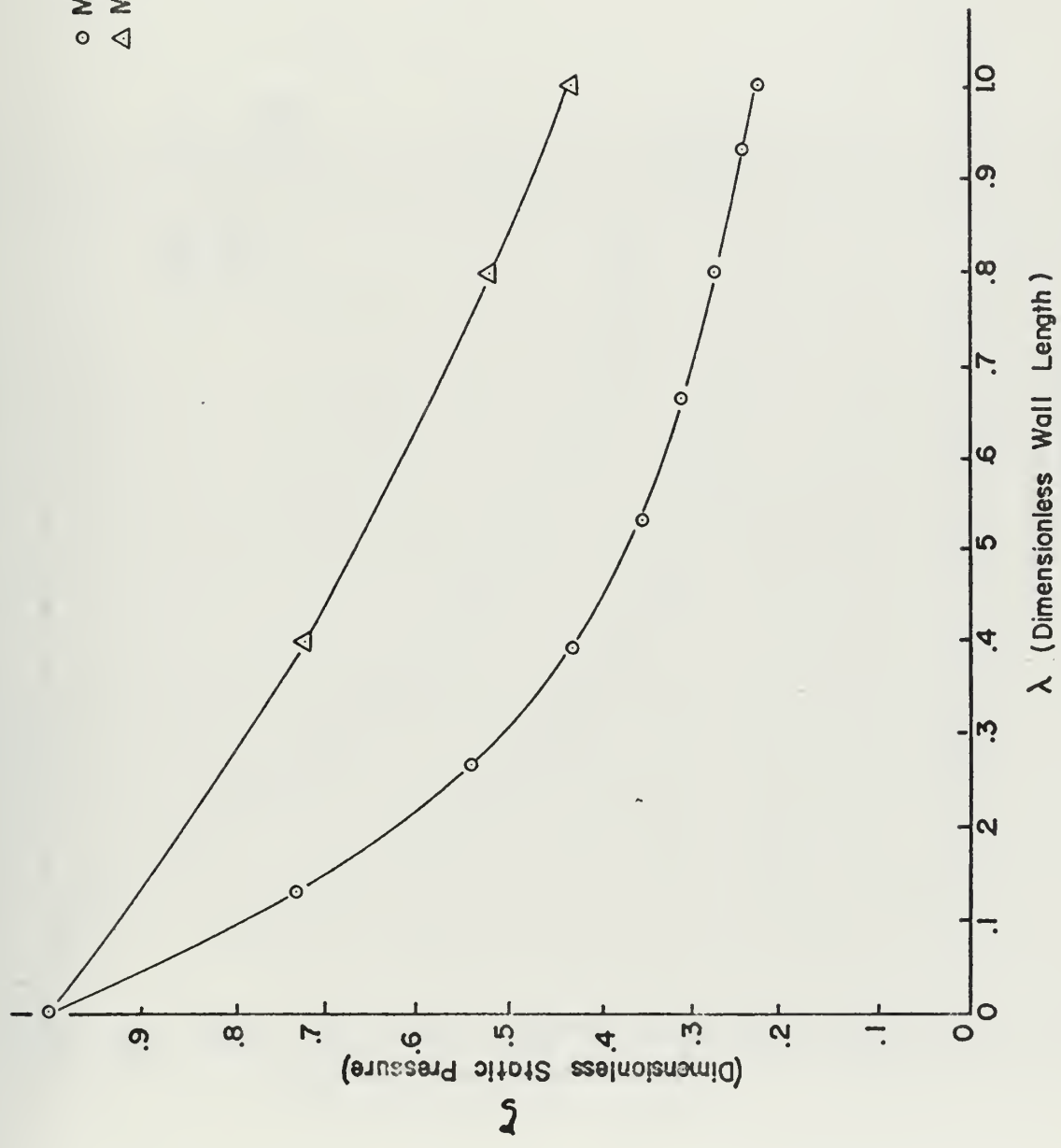


FIGURE 20

Dimensionless pressure distribution along outer wall of Model (1)

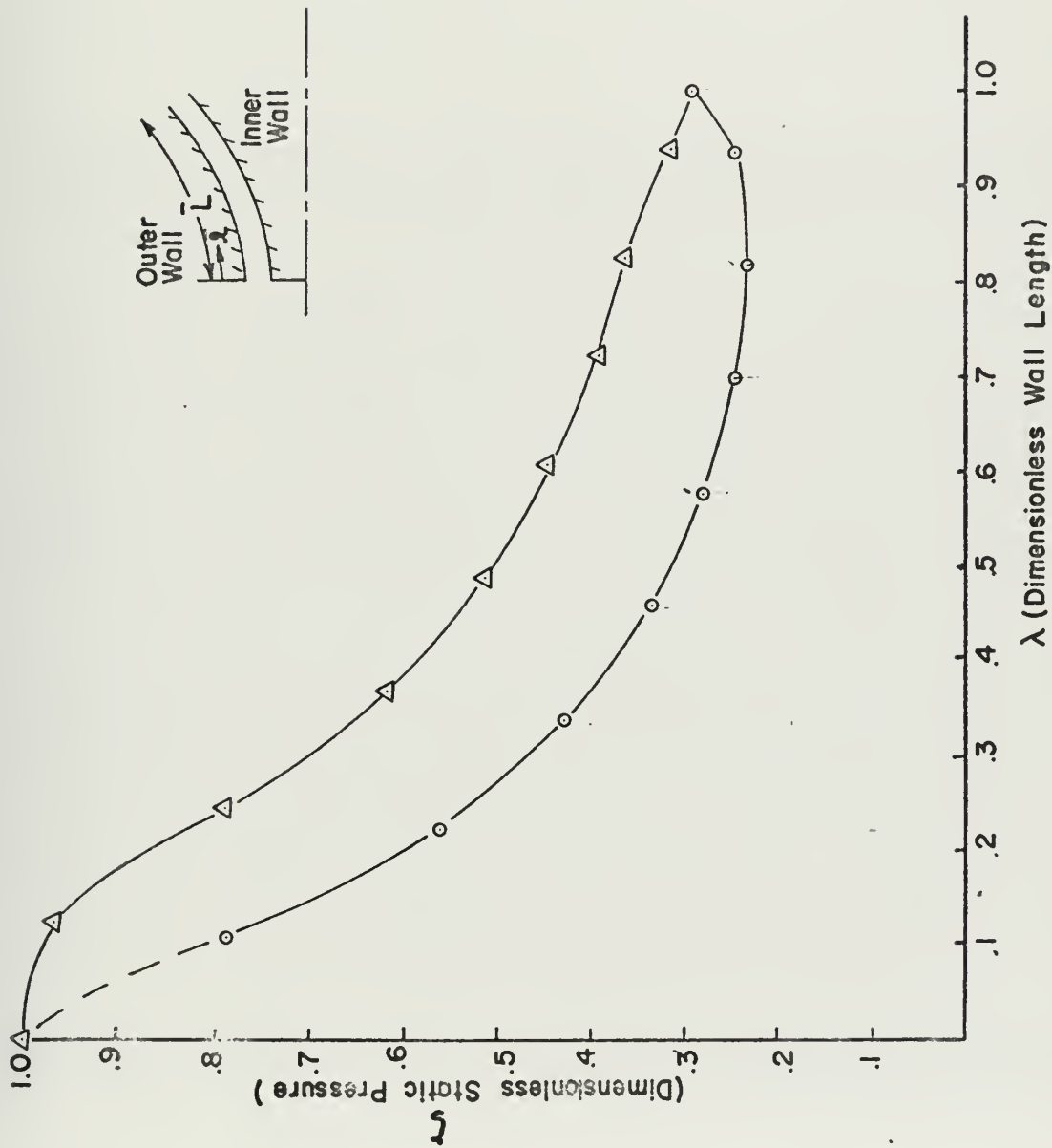


FIGURE 21

Dimensionless pressure distribution along the inner and outer walls of Model (2)

$$\zeta = \frac{P_{t1} - P_w}{q_1}$$

$$\lambda = \frac{\bar{r}}{L}$$

△ Outer Wall

○ Inner Wall (Center Piece)

meridional wall length. Values for ζ , λ , and p_w are contained in Table III, for the outer wall of Model (1) and for both the inner and outer walls of Model (2). The static pressure became higher than the ambient pressure at about $\lambda = 0.5$ on the inner wall of Model (2), which gives a ζ less than that at the exit. The value of ζ reaches a minimum between $\lambda = 0.7$ and $\lambda=0.9$ and increases again toward $\zeta = 0.293$ at the exit plane. This condition may be due to a separation of the flow, and indicates the need for proper wall contouring in addition to satisfying the criterion of Ω .

TABLE III

Meridional, static pressure values for Model (1) and Model (2)

CONTOUR	STATION	λ^*	p_w (in. water) gage	ζ^{**}
OUTER CONFIG. 1 Model (1)	1	0.0	-13.54	1.0
	2	0.133	- 8.79	0.729
	3	0.267	- 5.46	0.540
	4	0.400	- 3.50	0.429
	5	0.533	- 2.24	0.357
	6	0.667	- 1.45	0.312
	7	0.800	- 0.82	0.276
	8	0.933	- 0.34	0.249
	9	1.000	0.0	0.230
OUTER CONFIG. 4 Model (1)	1	0.0	- 9.66	1.0
	2	0.4	- 4.90	0.720
	3	0.8	- 1.45	0.520
	4	1.0	0.0	0.435

* λ - The dimensionless length \bar{l}/\bar{L}_w ** ζ - Dimensionless pressure

TABLE III, continued

CONTOUR	STATION	λ	p_w (in. water)	ζ
INNER Model (2)	2	0.107	-7.97	0.787
	3	0.222	-4.27	0.558
	4	0.336	-2.14	0.426
	5	0.460	-0.61	0.331
	6	0.578	+0.21	0.280
	7	0.697	+0.73	0.248
	8	0.817	+1.01	0.231
	9	0.933	+0.85	0.241
	10	1.000	0.00	0.293
OUTER Model (2)	1	0.0	-11.41	1.000
	2	0.121	-10.91	0.969
	3	0.241	-7.90	0.783
	4	0.366	-5.18	0.614
	5	0.484	-3.50	0.510
	6	0.605	-2.40	0.442
	7	0.718	-1.58	0.391
	8	0.823	-1.15	0.364
	9	0.938	-0.37	0.316
	10	1.000	0.00	0.293

VII. CONCLUSIONS AND RECOMMENDATIONS

This paper presents a design parameter Ω , for diffuser designs, which takes into account losses due to the geometry of the diffuser. It is shown from reference data and model tests that there is an abrupt increase in losses for diffusers designed for a value of Ω less than about five, and that this effect is independent of Reynolds number.

The parameter Ω is defined for incompressible, adiabatic flows. It is recommended that further experiments be made to extend the data for incompressible flows to higher values of Ω , and that an investigation of the compressible case be made.

It is suggested that Model (2) be improved by recontouring the inner wall to avoid separation. It is recommended also that the present inner contour be cut off at the station where the value of ζ is a minimum. Addition of static pressure taps on the inner wall at the inlet plane and a method for surveying the exit plane would provide data to better describe the flow.

It is recommended that the method of measuring pressure be investigated and improved to give more precise results for small, fluctuating pressure measurements, prior to conducting further tests on diffusers with $\Omega \bar{c}_f$ approaching zero.

APPENDIX A

DETERMINATION OF DIFFUSER EFFICIENCY

The diffuser efficiency was determined by the method of Vavra [10] for an adiabatic compression process with friction. The polytropic efficiency is defined for the differential compression from p to $p + \Delta p$ of Figure 3 as

$$\eta_p \equiv \frac{dT_{is}}{dT} \quad (A1)$$

The dimensionless flow function Φ_c and the relation for the polytropic exponent, n , from Ref. 10 are

$$\Phi_c = \dot{w} \sqrt{\frac{R}{g_c}} T_1 \frac{1}{p_1 A_2} = \sqrt{\frac{2\gamma}{\gamma-1} \left[\frac{T_{t1}}{T_1} \left(\frac{p_2}{p_1}\right)^{2/n} - \left(\frac{p_2}{p_1}\right)^{\frac{n+1}{n}} \right]} \quad (A2)$$

and

$$n = \frac{\gamma \eta_p}{1 - \gamma (1 - \eta_p)} \quad (A3)$$

where \dot{w} , T_{t1} , T_1 , p_2 and p_1 are either measured or computed for the particular diffuser design.

For an incremental change in pressure from p_1 to p_2 , the pressure p_2 may be expressed as $p_1 + \Delta p$, where Δp is small with respect to p_1 . The pressure ratios in (A2) can be expressed as

$$\frac{p_2}{p_1} = \left(1 + \frac{\Delta p}{p_1}\right) \quad (A4)$$

By the binominal expansion theorem,

$$\left(\frac{p_2}{p_1}\right)^{2/n} = \left(1 + \frac{\Delta p}{p_1}\right)^{2/n} = 1 + \frac{2}{n} \frac{\Delta p}{p_1} + \dots \quad (A5)$$

and similarly

$$\left(\frac{p_2}{p_1}\right)^{\frac{n+1}{n}} = 1 + \frac{n+1}{n} \frac{\Delta p}{p_1} + \dots \quad (A6)$$

and by assuming Δp to be small, the $(\Delta p/p_1)^2$ and higher order terms are much smaller than $\Delta p/p_1$ and are omitted.

From (A2)

$$\phi_c^2 \frac{\gamma-1}{2\gamma} = \frac{T_{t1}}{T_1} \left(\frac{p_2}{p_1}\right)^{2/n} - \left(\frac{p_2}{p_1}\right)^{\frac{n+1}{n}} \quad (A7)$$

Substituting expressions (A5) and (A6), and solving for n , gives

$$n = \frac{\frac{\Delta p}{p_1} \left[2 \frac{T_{t1}}{T_1} - 1 \right]}{\frac{\gamma-1}{2\gamma} \phi_c^2 - \frac{T_{t1}}{T_1} + 1 + \frac{\Delta p}{p_1}} \quad (A8)$$

Equating (A3) and (A8) gives

$$\eta_p = \frac{\frac{\Delta p}{p_1} \left[2 \frac{T_{t1}}{T_1} - 1 \right]}{\frac{\gamma}{\gamma-1} \left(\frac{T_{t1}}{T_1} - 1 \right) \left(2 \frac{\Delta p}{p_1} + 1 \right) - \frac{\phi_c^2}{2}} \quad (A9)$$

with

$$\frac{T_{t1}}{T_1} = 1 + \frac{\gamma-1}{2} M_1^2 \quad (A10)$$

the polytropic efficiency is

$$\eta_p = \frac{2 \frac{\Delta p}{p_1} \left[1 + (\gamma-1) M_1^2 \right]}{\phi_c^2 - \gamma M_1^2 \left[2 \frac{\Delta p}{p_1} + 1 \right]} \quad (A11)$$

APPENDIX B

DESIGN OF DIFFUSER MODEL (2)

From the results of Ref. 2 and the test data of Model (1), a design point of $\Omega \doteq 6$ and $\bar{L}/\Delta R \doteq 6$ was chosen from Fig. 18 for Model (2). The inlet area of Model (2) was the same as for Model (1).

From equation (42) of the main text,

$$C_{pri} - C_{pr} = \Omega \bar{c}_f$$

or, from equation (40), and a value of $\Omega \bar{c}_f = 0.1$,

$$\left[1 - \left(\frac{A_1}{A_2} \right)^2 \right] = 0.1 + C_{pr} \quad (B1)$$

For the range of C_{pr} from 0.65 to 0.72 for a $\bar{L}/\Delta R \doteq 6$, equation (B1) gives

$$A_2 = \frac{A_1}{1 - (0.1 + C_{pr})} \quad (B2)$$

giving a range of A_2 from 39 to 51 in².

An approximate radius was chosen to give a reasonable axial opening at a radial exit plane for $A_2 \doteq 45$ in².

Since the outer surface, E, of Fig. 22 was most critical from the standpoint of flow separation, it was designed first. A smooth curve of the desired shape was sketched in for surface E. To approximate the curve sketched, a series of circular arcs were constructed which provide for simple tooling layouts.

Figure 23 shows the method by which two circular arcs are fitted to satisfy the condition that both have centers on the same line at their tangent point (4), and that they fit into a given length, L.

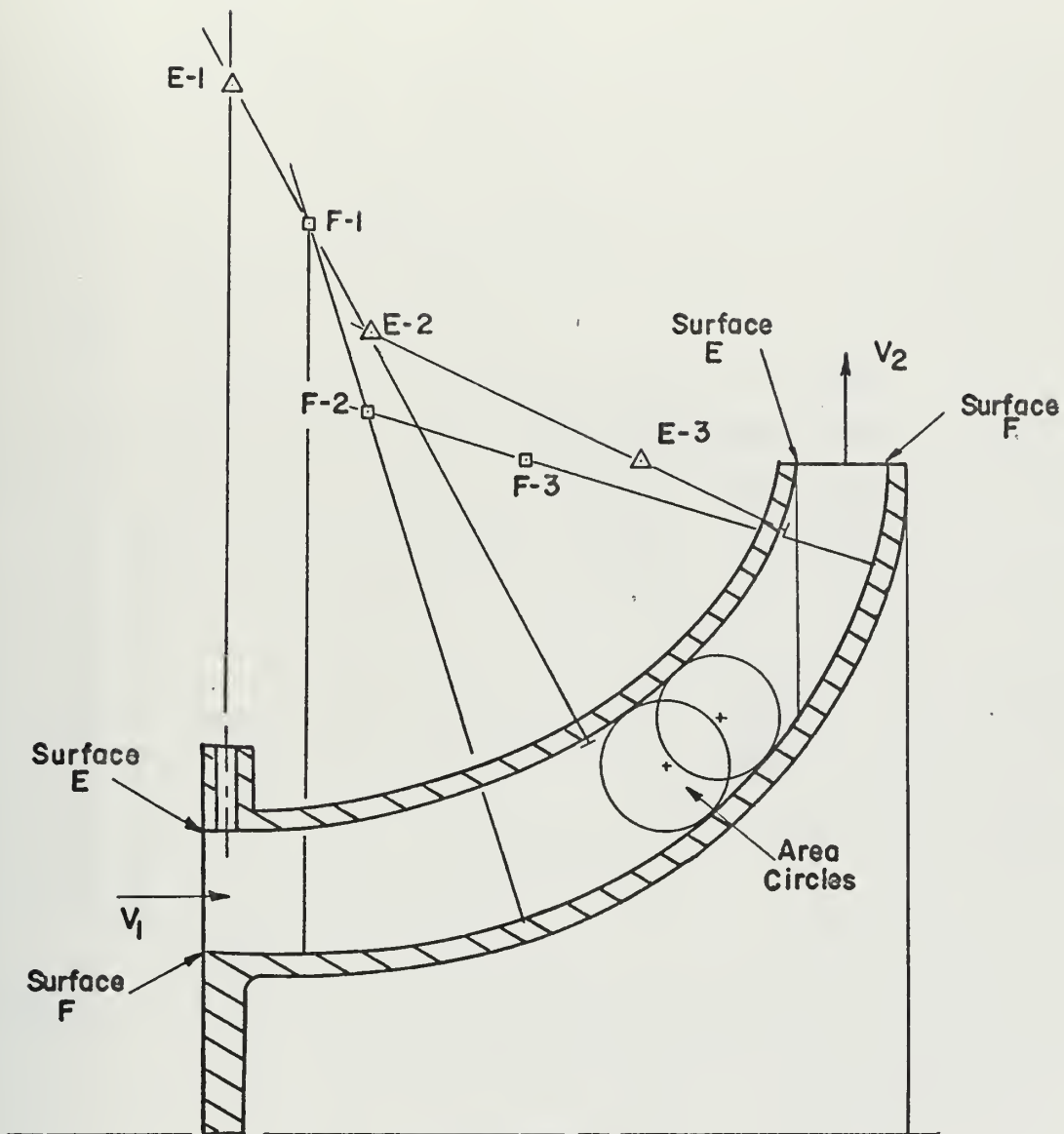


FIGURE 22
Design of Model (2)

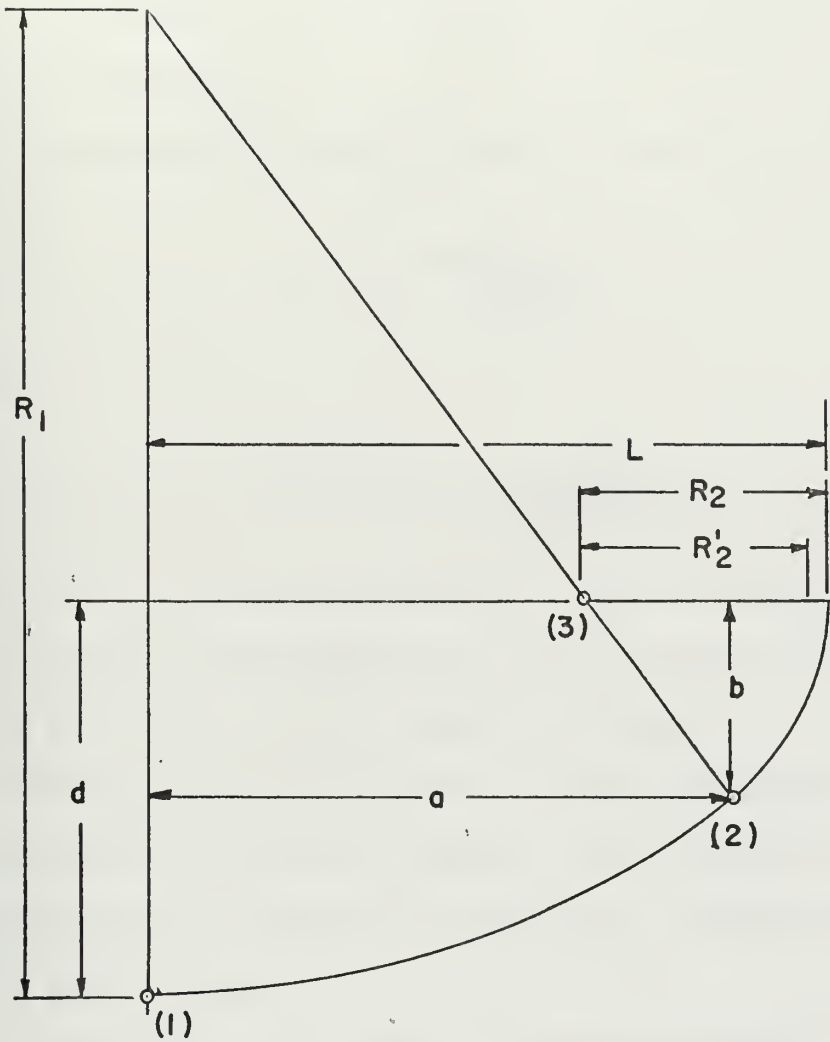


FIGURE 23
Fitting of circular arcs

The largest radius, R_1 , is chosen to give the desired effect of the original sketch. A curve is then drawn from point (1) to point (2), where (2) is an approximate point of the desired curvature change. Point (2) defines a and b for any given distance d. The center of R_2 becomes point (3).

From geometry, R_2 and R'_2 can be defined as

$$R_2 = \frac{b}{\sqrt{1 - (a/R_1)^2}} \quad (B3)$$

and

$$R'_2 = L - a \sqrt{\frac{ab}{R_1^2 - a^2}} \quad (B4)$$

Point (2) may be iterated until $R_2 = R'_2$. The centers of R_1 and R_2 will then be on the same radius at their tangent point and the curve will fall within the axial length L and height d.

The same procedure as described above was extended to surfaces of more than two circular arc segments, such as surface E, of Fig. 19, by locating the arc centers E-1, E-2, and E-3. Surface F was constructed in a similar manner.

With areas A_1 and A_2 known, a linear distribution of flow area from station (1) to station (2) was chosen. Circles of the diameter which gave the desired area at a given meridional station were then constructed along an approximate mean streamline as shown by the example circles on Fig. 22. Surface B was then sketched in, tangent to the area circles, and fitted with circular arcs as described above. The flow channel was then checked for uniformly increasing area as a function of length, and adjusted to prevent any convergence in the flow area.

APPENDIX C

COMPUTER PROGRAM OMEGA

Program "Omega" is a modification of program "Diffuser" used by Beck [6]. The program is written in Fortran IV for the IBM 360-67 digital computer. The program was established to compute the values of flow rate, Re , Ω , $\Omega \bar{c}_f$ and η_p by the methods described in the main text. Table C1 is a listing of the program.

C1. Assembly of Input Data

The field specifications for the input data are shown in Fig. 24. Card one of the data deck is a 72 space "Hollerith" statement for data identification. The content of this card is printed immediately below the output title. Card two is a two digit I-format number indicating the number of data points in the deck. Card three is the input of inlet and exit diameters and the value of Ω . Cards four and five contain the data recorded for one data point and must be repeated for each point. No other cards need be repeated.

All floating point numbers may be placed anywhere in their field. I-format numbers must be right justified.

The definitions of the program input variables are given below.

<u>Fortran Symbol</u>	<u>Definition</u>	<u>Format</u>
NUM	Number of sets of data points	I 2
D01	Diameter of outer wall station one	F 10.0
D11	Diameter of inner wall station one	F 10.0
D02	Diameter of outer wall station two	F 10.0

<u>Fortran Symbol</u>	<u>Definition</u>	<u>Format</u>
DO2	Diameter of outer wall, station two	F 10.0
DI2	Diameter of inner wall, station two	F 10.0
OMEGA	Value of shape parameter	F 10.0
IRUN	Number of run	I 3
MO	Month	I 3
IDAY	Day	I 3
PATM	Atmospheric pressure	F 10.0
PINOZ	Static pressure upstream of nozzle	F 10.0
DPNOZ	Pressure differential across nozzle	F 10.0
TNOZ	Total temperature upstream of nozzle	F 10.0
TEMP	Temperature read at barometer	F 10.0
P1	Static pressure at station one	F 10.0
Q1	Dynamic head at station one	F 10.0
TT1	Total temperature measured upstream of station one	F 10.0
TRM	Ambient room temperature at exit	F 10.0

C2. Output

The program output is in three sections. The first section is a printout of data as read from the input cards as a check. The second section is the calculation of flow rate which is divided into input values converted by the program to dimensionally correct units, and output of flow rates computed by the program. The third section is also divided into input values converted by the program and output values of interest in evaluation of diffuser performance.

Table C2 is a sample output of the program.

CARD

1	72	
72 Space Hollerith Statement		
Data Identification		Blank

CARD 2

1 2	
I 3	
NUM	Blank

CARD 3

1	10	11	20	21	30	31	40	41	50	
F10.0		F10.0		F10.0		F10.0		F10.0		
D01		DI1		D02		DI2		OMEGA		Blank

CARD 4

1	3	4	6	7	9	10	19	20	29	30	39	40	49	50	59	
I 3		I 3		I 3		F10.0		F10.0		F10.0		F10.0		F10.0		
IRUN		MO		IDAY		PATM		PINOZ		DPNOZ		TNOZ		TEMP		Blank

CARD 5

1	10	11	20	21	30	31	40	
F10.0		F10.0		F10.0		F10.0		
P1		Q1		TT1		TRM		Blank

FIGURE 24

Input field specifications for Program Omega

TABLE C1

Listing of Program Omega

```

CCC
ASSIGN VALUES TO FIXED CONSTANTS NEEDED FOR COMPUTATIONS
TSTD=518.7
PSTD=29.92*.4912
TEXAS=.8
CE=32.174
R=53.35
GM=1.4
MM=0

CCC
READ IN INPUT DATA AND PRINT OUT FOR DATA CHECK
READ (5,1000) NUM
READ (5,10) DO1,DI1,DO2,DI2,OMEGA
READ (5,30) IRUN,MO,IDAY,PATM,PINO7,DPNO7,TNOZ,TEMP
15 READ (5,25) PI,Q1,TTL,TRM
NM=MM+1
WRITE (6,399)
WRITE (6,400)
WRITE (6,1000) IRUN,MO,IDAY
WRITE (6,401)
WRITE (6,380)
WRITE (6,381)
WRITE (6,382) PI,Q1,TTL,TRM

CCC
CONVERT DATA INTO DIMENSIONALLY CORRECT UNITS OF MEASURE
TEMP=(5./9.)*(TEMP-32.)
PATM=PATM*(1.-((.0001634*TEMP)/(1.+0.0001818*TEMP)))*.4912
P2=PATM
DPNOZ=DPNOZ*TEXAS*.03613
PINOZ=PATM+PINO7*TEXAS*.03613
Q1=Q1*TEXAS*.03613
P1=PATM+P1*.03613*TEXAS
P1=P1+Q1
TTL=32.174+35.77*TTL-.4518*TTL**2
TTL=P1+459.7
TNOZ=32.174+35.77*TNOZ-.4518*TNOZ**2
TNOZ=P1+459.7

```


TABLE C1, continued

```

C
C
C BEGIN FLOW RATE CALCULATIONS USING FLOW NOZZLE READINGS
C
C      X=DPNOZ/P1NOZ
C      Y=(1.-X)**1.428
C      Z=(1.-X)**0.286
C      EPS=SQRT(2.433*Y/X*(1.-Z)/(1.-.305*Y))
C      FT=1.+0.00015*(TNOZ-60.)
C      WEQIV=11.3*EPS*FT*SQRT(X)
C      WDOT=WEQIV*P1NOZ*SQRT(G/(R*TNOZR))
C
C      COMPUTE MACH NUMBER
C
C      AMACH=SQRT(2./((GAM-1.)*((PT1/P1)**((GAM-1.)/GAM)-1.)))
C
C      COMPUTE STATIC TEMPERATURE AT INLET
C
C      TIR=TTIR/(1.+(GAM-1.)/2.*AMACH**2)
C
C      COMPUTE THE DENSITY OF THE FLOW IN THE CENTRAL REGION
C
C      RO=P1*144./(R*G*TIR)
C
C      COMPUTE THE COEFFICIENT OF PRESSURE RECOVERY
C
C      CPR=(P2-P1)/Q1
C
C      COMPUTE REYNOLDS NUMBER TIMES 10**-7
C
C      RE=WDOT*12./(3.14159*4.998*3.9*G)
C
C      COMPUTE THE IDEAL COEFFICIENT OF PRESSURE RECOVERY
C
C      RT1=DO1/2.
C      RH1=DI1/2.
C      RT2=DO2/2.
C      RH2=DI2/2.
C      A1=3.14159*(RT1**2-RH1**2)
C      A2=2.*3.14159*RT2*1.
C      CPrI=1.-((A1/A2)**2)
C
C      COMPUTE THE REFERRED FLOW RATE (NORMALIZED TO STANDARD DAY
C      CONDITIONS)
C
C      TRM=TRM+459.7
C      WSTD=WDOT*SQRT((TRM/TSTD)/(PATM/PSTD))
C
C      COMPUTE THE POYTROPIC EFFICIENCY

```


TABLE C1, continued

```

413 FORMAT (15X, 'DIFFUSOR PERFORMANCE DATA'//)
414 FORMAT(25X, 'ATMOSPHERIC PRES. =', F8.4, ' PSI ', 11X, ' COEF. OF PRE
ISSUE RECOVERY =', F9.4)
415 FORMAT (25X, 'P1 (INLET STATIC) =', F8.4, ' PSIA', 12X, ' INLET CONDIT
IONS: ')
416 FORMAT (25X, 'PT1 (INLET TOTAL) =', F8.4, ' PSIA')
417 FORMAT (25X, 'P2 (EXIT STATIC) =', F8.4, ' PSIA', 12X, ' DENSITY
(CENTRAL CORE) =', F9.4, ' SLUGS/CU FT')
418 FORMAT (76X, 'REYNOLDS NO. (X 10**7) =', F9.4)
419 FORMAT (76X, 'MACH NO. (INLET CORE) =', F9.4)
420 FORMAT (71X, 'POLYTROPIC EFFICIENCY =', F9.4)
421 FORMAT (71X, 'OMEGA =', F9.4)
423 FORMAT (71X, 'IDEAL RECOVERY COEF. =', F9.4)
424 FORMAT (71X, 'OMEGA TIMES CFBAR =', F9.4)
425 FORMAT (71X, 'COEF. OF FRICTION(CFBAR) =', F9.4)
1000 1
      1
      )
      END

```


TABLE C2

SAMPLE OUTPUT OF PROGRAM OMEGA

ANNULAR DIFFUSER PERFORMANCE EVALUATION DATA

DIFFUSER MODEL (2) OMEGA=5.701

RUN 15

DATE 5-22-70

DATA CHECK

PATM=29.900 P1NOZ=78.600 PPN07=122.800 TNOZ= 1.73 TEND=51.00 DEG F
P1= -14.260 O1=20.175 T1= 1.72 TPE=26.00

FLOW RATE, MEASURED WITH 3.022 INCH FLOW NOZZLE

INPUT:

P1(NOZZLE) = 16.8995 PSIA
DELTA PRESSURE = 2.5783 PSIA
TOTAL TEMPERATURE = 92.6738 DEG F

OUTPUT:
FLOW RATE (MASS) = 2.4085 LB/SEC
EQUIVALENT FLOW RATE = 4.3132 SQ. IN.
REFERED FLOW RATE = 2.4930 LB/SEC

DIFFUSOR PERFORMANCE DATA

INPUT:

ATMOSPHERIC PRES. = 14.6219 PSI
P1 (INLET STATIC) = 14.2087 PSIA
P2 (EXIT STATIC) = 14.6219 PSIA

OUTPUT:

COEFF. OF PRESSURE RECOVERY = 0.7049
INLET CONDITIONS:
DENSITY (CENTRAL CORE) = .2164E-02
REYNOLDS NO. (X 10**-7) = .1447E-01
MACH NO. (INLET CORE) = 0.2406
POLYTROPIC EFFICIENCY = 0.9924
OMEGA = 5.7010
IDEAL PRES. RECOVERY COEFF. = 0.8017
OMEGA TIMES CERAP = 0.0649
COEFF. OF FRICTION (CFRFR) = 0.0165

SLUGS/CU FT

APPENDIX D

REDUCTION OF DATA FROM SOVRAN AND KLOMP, REFERENCE 2

Data of Ref. 2 were reduced by a Fortran IV program to a form useable for this study. Table D1 is a listing of the program. The diffuser description of Ref. 2 was the same as in Fig. 10.

The definition of the input variables are

<u>Fortran Symbol</u>	<u>Description</u>
ALFAH	The divergence angle, α_H , of the inner wall
ALFAT	The divergence angle, α_T , of the outer wall
DIMLL	The dimensionless length, $\bar{L}/\Delta R$.
ARATIO	Area ratio, A_2/A_1
RRATIO	Radius ratio, R_{H1}/R_{T1}
RT1	Radius of outer wall, station one
CPR	Coefficient of pressure recovery

The axial length was computed from the geometry and a numerical integration was made to obtain Ω . The ideal pressure recovery coefficient was computed from the area ratio and used to compute $\Omega \bar{c}_f$. The results are contained in Table D2, where

<u>Fortran Symbol</u>	<u>Description</u>
OMEGA	The shape parameter, Ω
CFBAR	Average local coefficient of friction, \bar{c}_f
DIMLL	The dimensionless length, $\bar{L}/\Delta R$
OCF	The product, $\Omega \bar{c}_f$

TABLE D1

Listing of reference data reduction program

```

C COMPUTE OMEGA AND CFBAR FOR CIRCULAR, ANNUAL DIFFUSERS
3 WRITE (6,1)
1 FORMAT ('IHI/////////20X,'SOVRAN & KLOMP, GMR-511, DATA',////)
I=1
5 READ (5,10) ALFAH,ALFAT,DIMLL,ARATIO,RRATIO,RT1,CPR,PT,IDENT
10 FORMAT ('F10.0,A5,I5)
C CONVERT TO RADIANS
V=ALFAT/57.29577
W=ALFAH/57.29577
A=RT1*(1.+RRATIO)
B=TAN(V)+TAN(W)
C=RT1*(1.-RRATIO)
D=RT1**2*(1.-RRATIO**2)
E=TAN(V)-TAN(W)
C CONVERTING DIMLL TO ACTUAL LENGTH FOR CASES USING LBAR
P=COS(V)
Q=COS(W)
F=2.*DIMLL*C*(ARS(P)*ABS(Q)/(ABS(P)+ABS(Q)))
X=(A+E-C*B)
Y=(A+B**F)
Z=(C+E**F)
OMEGA=(D**2/X)*(-1./(Y*Z**2)-3.*B*((1./X)*(-1./(Y*Z)-2.*B*((1./X)*2(1./Y+(E/X)*ALOG(Z/Y)))))-((-1./A*(A**2))-3.*B*((1./X)*(-1./A*(A**2)*P*(1./X)*(-1./A+(E/X)*ALOG(C/A))))))
CPR=1.-((1./ARATIO**2)
OCF=CPRI-CPRI-CPR
CFBAR=OCF/OMEGA
WRITE (6,20) OMEGA,CFBAR,DIMLL,OCF
20 FORMAT ('15X,F10.4)
I=I+1
IF(I.GT.50) GO TO 3
IF(IDENT.LT.1) GO TO 5
END

```


TABLE D2

SOVRAN & KLUMP, GMR-511, DATA

OMEGA	CFBAR	DIMLL	OCF
3.6454	0.0027	2.2800	0.0097
5.2663	0.0054	3.6300	0.0283
7.2076	0.0117	5.6600	0.0841
9.1634	0.0125	8.3700	0.1146
9.9462	0.0136	9.7200	0.1351
10.6331	0.0137	11.0700	0.1461
11.5207	0.0132	13.1000	0.1519
3.6454	0.0013	2.2800	0.0047
7.2076	0.0119	5.6600	0.0861
7.2076	0.0124	5.6600	0.0891
7.2076	0.0143	5.6600	0.1031
9.1634	0.0135	8.3700	0.1236
9.1634	0.0143	8.3700	0.1306
11.5207	0.0147	13.1000	0.1689
2.9639	0.0221	2.2600	0.0655
3.4199	0.0345	2.9300	0.1181
3.7999	0.0291	3.6100	0.1105
4.4838	0.0369	4.9600	0.1656
4.5598	0.0291	5.6400	0.1328
4.6358	0.0406	6.3200	0.1884
5.0918	0.0391	8.2400	0.1993
5.3198	0.0372	10.3700	0.1978
5.5478	0.0388	13.0800	0.2151
2.9639	0.0262	2.2600	0.0775
3.7999	0.0306	3.6100	0.1165
3.7999	0.0391	3.6100	0.1485
3.7999	0.0375	3.6100	0.1425
3.7999	0.0388	3.6100	0.1475
3.7999	0.0430	3.6100	0.1635
4.5598	0.0296	5.6400	0.1348
4.5598	0.0344	5.6400	0.1568
4.5598	0.0368	5.6400	0.1678
4.5598	0.0421	5.6400	0.1918
2.7142	0.0511	2.2500	0.1387
3.1363	0.0575	2.9300	0.1804
3.4570	0.0631	3.6000	0.2182
2.4240	0.0957	2.2400	0.2320
2.7430	0.1057	2.9100	0.2900
2.9811	0.1098	3.5900	0.3274
3.4800	0.1070	6.2900	0.3722
3.7044	0.1046	9.6800	0.3875
3.7914	0.0983	13.0600	0.3728
2.7884	0.0518	2.2600	0.1444
2.9829	0.0547	2.7100	0.1633
3.0478	0.0570	3.0500	0.1736
3.3071	0.0551	3.4000	0.1856
3.5017	0.0556	3.7500	0.1949
3.6314	0.0514	4.4400	0.1866
3.8908	0.0471	5.1400	0.1833
4.1501	0.0427	5.8300	0.1772

TABLE D2, continued

SOVRAN & KLOMP, GMR-511, DATA

OMEGA	CFBAR	DIMLL	OCF
2.7884	0.0582	2.3600	0.1624
2.9829	0.0624	2.7100	0.1863
2.2947	0.1408	2.3400	0.3231
2.4358	0.1429	2.6800	0.3480
2.5578	0.1468	3.0300	0.3756
2.6602	0.1484	3.3800	0.3949
2.7467	0.1515	3.7200	0.4163
2.8820	0.1484	4.4200	0.4276
2.9835	0.1445	5.1200	0.4305
3.0580	0.1397	5.8000	0.4273
2.1696	0.1691	2.3300	0.3669
2.2974	0.1723	2.6800	0.3959
2.4030	0.1738	3.0300	0.4177
2.4886	0.1761	3.3700	0.4382
2.5627	0.1768	3.7200	0.4530
1.9748	0.2188	2.3200	0.4321
2.0752	0.2247	2.6600	0.4662
2.1593	0.2278	3.0100	0.4919
2.2281	0.2309	3.3600	0.5146
2.2851	0.2322	3.7100	0.5305
2.4784	0.2310	5.7900	0.5725
2.8590	0.0378	2.4200	0.1081
3.8475	0.0298	3.9200	0.1147
4.7895	0.0249	6.1100	0.1190
5.5813	0.0210	9.1700	0.1172
1.8581	-0.0030	1.4300	-0.0057
2.4553	0.0153	2.3000	0.0376
3.0217	0.0276	3.6000	0.0833
3.4734	0.0328	5.3400	0.1139
1.8581	-0.0036	1.4300	-0.0067
1.8581	0.0126	1.4300	0.0233
2.4553	0.0124	2.3000	0.0306
3.0217	0.0226	3.6000	0.0683
3.4734	0.0230	5.3400	0.0799
3.4734	0.0269	5.3400	0.1280
2.3698	-0.0155	1.4700	-0.0368
3.3697	-0.0057	2.3400	-0.0191
4.4930	-0.0012	3.6400	-0.0053
5.5348	0.0037	5.3800	0.0206
2.3698	-0.0109	1.4700	-0.0258
5.5348	0.0102	5.3800	0.0566
1.6569	-0.0004	1.5000	-0.0006
1.8824	0.0001	1.9500	0.0002
2.0503	0.0003	2.4000	0.0006
2.1776	0.0000	2.8500	0.0000
2.2757	-0.0002	3.3000	-0.0004
2.3525	0.0001	3.7500	0.0002
2.4134	0.1735	4.2000	0.4186
2.4631	0.1723	4.6600	0.4244
2.5024	0.1725	5.1100	0.4316

TABLE D2, continued

SOVRAN & KLUMP, GMR-511, DATA

OMEGA	CFBAR	DIMLL	OCF
2.5346	0.1732	5.5600	0.4390
1.6569	0.1409	1.5000	0.2334
2.5346	0.1846	5.5600	0.4680
2.8154	0.0021	2.0100	0.0058
3.5666	0.0045	2.8600	0.0162
4.2207	0.0108	3.8100	0.0457
4.7081	0.0122	4.7100	0.0574
5.4215	0.0135	6.5200	0.0734
5.6828	0.0135	7.4200	0.0768
5.8977	0.0120	8.3100	0.0705
2.8154	0.0038	2.0100	0.0108
2.8053	0.0067	2.0000	0.0188
1.4279	0.2348	1.5600	0.3353
1.5757	0.3059	2.0200	0.4820
1.6803	0.3143	2.4900	0.5281
1.7532	0.3205	2.9500	0.5619
1.8075	0.3232	3.4200	0.5841
1.8472	0.3242	3.8800	0.5989
1.4279	0.2313	1.5600	0.3303
1.8472	0.3291	3.8800	0.6079
2.2047	0.1129	2.0800	0.2488
2.4275	0.0844	2.5400	0.2048
2.8579	0.0903	3.9300	0.2582
2.2047	0.1201	2.0800	0.2648
2.8579	0.1113	3.9300	0.3182

BIBLIOGRAPHY

1. Gleason, J. G., An Investigation of Current Subsonic Diffuser Design Knowledge with Emphasis on Jet Engine Annular Diffusers, a Pratt and Whitney Summer Faculty Program Project, Summer 1963.
2. General Motors Research Publication GMR 511, Experimentally Determined Optimum Geometrics for Rectilinear Diffusers with Rectangular, Conical or Annular Cross-Section, by Gino Sovran and E. D. Klomp, 16 November 1965.
3. Vavra, M. H., AGARD Lecture Series 39, Lecture Series on Basic Elements for Advanced Designs of Radial-Flow Compressors, June 1970.
4. Vavra, M. H., von Karman Institute, Course Note, Lecture Series on Flow in Radial Compressors, June 1967.
5. Kelly, R. J., An Investigation of the Oxidizer Flow Passages in a Dual-Combustion Liquid Rocket Engine, Engineer's Thesis, Naval Postgraduate School, September 1967.
6. Beck, G. L., An Experimental Determination of Two-Dimensional Ribbed Wall Diffuser Performance, Master's Thesis, Naval Postgraduate School, March 1968.
7. Eshback, Ovid W., Handbook of Engineering Fundamentals, Second Edition, New York, John Wiley and Sons, Inc., 1965.
8. Shenker, H., Reference Tables for Thermocouples, National Bureau of Standards, United States Department of Commerce, Circular 561.
9. Koch, R., and Feind, K., Druckverlust und Wärmeübergang in Ringspalten, Chemie Ingenieur Technik, Vol. 30, 1958.
10. Vavra, M. H., von Karman Institute, Course Note 54a, Part 1, Lecture Series on Problems of Fluid Mechanics in Radial Turbomachines, March 1965.

INITIAL DISTRIBUTION LIST

	No. Copies
1. Defense Documentation Center Cameron Station Alexandria, Virginia 22314	2
2. Library, Code 0212 Naval Postgraduate School Monterey, California 93940	2
3. Chairman, Department of Aeronautics Naval Postgraduate School Monterey, California 93940	1
4. Professor M. H. Vavra Department of Aeronautics Naval Postgraduate School Monterey, California 93940	3
5. Professor R. D. Zucker Department of Aeronautics Naval Postgraduate School Monterey, California 93940	1
6. Lieutenant Donald R. Gapp 1934 Arizona Avenue Sturgis, South Dakota 57785	1

DOCUMENT CONTROL DATA - R & D

(Security classification of title, body of abstract and indexing annotation must be entered when the overall report is classified)

ORIGINATING ACTIVITY (Corporate author)

Naval Postgraduate School
Monterey, California 93940

2a. REPORT SECURITY CLASSIFICATION

Unclassified

2b. GROUP

REPORT TITLE

A Design Criterion for Arbitrary Diffusers

DESCRIPTIVE NOTES (Type of report and, inclusive dates)

Aeronautical Engineer, June 1970

AUTHOR(S) (First name, middle initial, last name)

Donald Robert Gapp

REPORT DATE

June 1970

7a. TOTAL NO. OF PAGES

82

7b. NO. OF REFS

10

9. CONTRACT OR GRANT NO.

b. PROJECT NO.

9a. ORIGINATOR'S REPORT NUMBER(S)

9b. OTHER REPORT NO(S) (Any other numbers that may be assigned this report)

10. DISTRIBUTION STATEMENT

This document has been approved for public release and sale;
its distribution is unlimited.

11. SUPPLEMENTARY NOTES

12. SPONSORING MILITARY ACTIVITY

Naval Postgraduate School
Monterey, California 93940

13. ABSTRACT

This study presents the derivation of a diffuser design parameter, which takes into account losses due to the geometry of the diffuser.

A criterion for design of annular diffusers, using the design parameter to predict losses, is developed from reference data and model tests.

A curved wall annular diffuser was designed and tested to verify the predictions of the design criterion for an arbitrary diffuser.

KEY WORDS	LINK A		LINK B		LINK C	
	ROLE	WT	ROLE	WT	ROLE	WT
Design criterion for arbitrary diffusers						
Diffusers						
Derivation of a diffuser design parameter						
Annular diffusers						
Arbitrary diffusers						
Losses in diffusers						



Thesis
G18
c.1

119310

Gapp

A design criterion
of arbitrary diffusers.

Thesis
G18
c.1

119310

Gapp

A design criterion
of arbitrary diffusers.

thesG18

A design criterion for arbitrary diffuse



3 2768 002 01034 0

DUDLEY KNOX LIBRARY